

The role of active site flexible loops in catalysis and of zinc in conformational stability of *Bacillus cereus* 569/H/9 β -lactamase

Caroline Montagner¹, Michaël Nigen^{1‡}, Olivier Jacquin¹, Nicolas Willet^{1◇}, Mireille Dumoulin¹, Andreas Ioannis Karsisiotis², Gordon C.K. Roberts³, Christian Damblon⁴, Christina Redfield⁵ and André Matagne¹

¹ Laboratoire d'Enzymologie et Repliement des Protéines, Centre d'Ingénierie des Protéines, Université de Liège, Institut de Chimie B6, 4000 Liège (Sart Tilman), Belgium

² School of Biological Sciences, University of Essex, Wivenhoe Park, Colchester, Essex CO4 3SQ, UK

³ Henry Wellcome Laboratories of Structural Biology, Department of Biochemistry, University of Leicester, Leicester LE1 9HN, United Kingdom

⁴ Département de Chimie, Université de Liège, Institut de Chimie B6, 4000 Liège (Sart Tilman), Belgium

⁵ Department of Biochemistry, University of Oxford, South Parks Road, Oxford, OX1 3QU, United Kingdom

‡ Present address: Montpellier SupAgro, UMII, CIRAD, INRA, UMR Ingn Agropolymères & Technologies Emergentes 1208, F-34060 Montpellier 01, France.

◇ Present address: Département de Chimie, Université de Liège, Liège, Belgium

Running title : Folding of BcII metallo- β -lactamase

To whom correspondence should be addressed: Prof. André Matagne, Laboratoire d'Enzymologie et Repliement des Protéines, Centre d'Ingénierie des Protéines, Université de Liège, Institut de Chimie B6, 4000 Liège (Sart Tilman), Belgium, Telephone : +32 (0)43663419 ; Email : amatagne@ulg.ac.be

Keywords: antibiotic resistance, metalloenzyme, β -lactamase, protein folding, nuclear magnetic resonance (NMR), circular dichroism (CD), zinc, enzyme catalysis.

ABSTRACT

Metallo- β -lactamases catalyse the hydrolysis of most β -lactam antibiotics and hence represent a major clinical concern. The development of inhibitors for these enzymes is complicated by the diversity and flexibility of their substrate binding sites, motivating research into their structure and function. In this study, we examined the conformational properties of the *Bacillus cereus* β -lactamase II in the presence of chemical denaturants using a variety of biochemical and biophysical techniques. The apoenzyme was found to unfold cooperatively,

with a Gibbs free energy of stabilization (ΔG°) of 32 ± 2 kJ·mol⁻¹. For holoBcII, a first non-cooperative transition leads to multiple interconverting native-like states, in which both zinc atoms remain bound in an apparently unaltered active site and the protein displays a well-organized compact hydrophobic core with structural changes confined to the enzyme surface, but with no catalytic activity. 2D NMR data revealed that the loss of activity occurs concomitantly with perturbations in two loops that border the enzyme active site. A second cooperative transition, corresponding to global unfolding, is observed at higher denaturant

concentrations, with ΔG° value of 65 ± 1.4 kJ·mol⁻¹. These combined data highlight the importance of the two zinc ions in maintaining structure as well as a relatively well-defined conformation for both active site loops in order to maintain enzymatic activity.

β -lactamases catalyse hydrolysis of the β -lactam ring of antibiotics belonging to the penicillin family (1-3). Synthesis of these enzymes represents the major cause of bacterial resistance to β -lactam antibiotics (4-7). They are classified into two structural superfamilies (8), namely the active-site serine enzymes (both β -lactamases and penicillin binding proteins) and the metallo- β -lactamases (MBLs). The latter, also referred to as class B β -lactamases, require one or two zinc ions for activity (9-11). They show no structural similarity with the active-site serine β -lactamases and they are part of a remarkable set of enzymes (i.e. the zinc metallo-hydrolase family of the β -lactamase fold or, more simply, the MBL superfamily (10-16)) that exhibit a wide variety of functions related to hydrolysis and redox reactions, and DNA and RNA metabolism. Seventeen groups of enzymes have been identified on the basis of their biological functions (13), which all share a novel $\alpha\beta/\beta\alpha$ fold. Most of the 3D structures reveal a binuclear centre with metal ligands located on loops connecting secondary structure elements (15,17).

Zinc β -lactamases have been found in many bacterial species, including pathogenic strains (18,19). Most of them are able to hydrolyse almost all β -lactam antibiotics (20,21), including carbapenems (i.e. a family of last resort β -lactams that generally escape the activity of the most widespread serine β -lactamases), and they are not sensitive to the classical inactivators of serine β -lactamases, such as clavulanate, sulbactam and tazobactam (22,23). Furthermore, these enzymes are often encoded by highly transmissible genetic elements (i.e. plasmids, transposons and integrons), which allow their spreading among pathogenic bacteria (5,6,18,24). Thus, MBLs have been reported to be of particular concern for public health (18;19;24-28) and the development of effective inhibitors of zinc β -lactamases to counteract the ongoing widespread resistance to β -

lactam antibiotics is of immediate clinical relevance. The structural diversity of the MBLs and the plasticity of their binding sites, at the level of both the zinc centre and the adjacent substrate binding loops, render the design of such compounds a difficult task (29). This will likely not be possible without a detailed understanding of both the mechanism of action of these enzymes and the interactions which determine the structure-activity relationships among MBL inhibitors (17,23,30,31). This is even more obvious in the light of the challenge of overcoming *in vivo* toxicity associated with cross reactivity with human metallo-enzymes (32).

MBLs are grouped according to sequence similarities and zinc coordination into subclasses B1, B2 and B3 (10,33). Enzymes from each class exhibit specific functional and mechanistic properties (34,35). In particular, while the B1 and B3 enzymes display maximum activity as dizinc species, the B2 β -lactamases are inhibited upon binding of a second zinc (36). The first class B enzyme was isolated from an innocuous strain of *Bacillus cereus* (37). This protein, known as BcII, is the archetype, most extensively studied model of enzymes of the largest, ubiquitous and clinically relevant B1 subclass, such as VIM-, IMP- and NDM-type MBLs (all transferable broad spectrum β -lactamases) (38). BcII consists of 227 residues in the mature form ($M_r = 24960/25088$ in the absence/presence of zinc ions) and its three dimensional structure (Figure 1, both X-ray crystal and solution NMR (31, 39-41)) exhibits the classical MBL fold, i.e. a four-layered $\alpha\beta/\beta\alpha$ structure, comprising a central β -sheet sandwich flanked on either side by two α -helices. The active site, with two zinc ions readily accessible to solvent, is located at the bottom of a long wide groove running on the surface of the protein, at one edge of the β -sheet sandwich. The shape of the active site cleft is modulated by conformational changes of two long loops { $\beta 3$ - $\beta 4$ [residues 32-38(59-66)] and $\beta 11$ - $\alpha 4$ [170-188(223-241)]}. {Residue numbering is presented as: number in BcII sequence(number in standard BBL system) (33,42) throughout the text, and all structural elements are defined according to the solution NMR structure (31)}. Note that these loops have also been widely referred to as L1 and L3, respectively.

BcII has been reported to be active in the presence of either one or two zinc ions at the active site, although maximum activity is observed with two zinc bound (20,43-45). However, Jacquin *et al.* (46) demonstrated that at 1:1 [Zn]/[BcII] ratio the only species present were apoenzyme and dizinc enzyme, indicating cooperative binding of the zinc ions and suggesting that the dizinc species is the only relevant form of the enzyme for activity (46). For dizinc MBLs, hydrolysis has been suggested to occur by cleavage of the amide bond of the β -lactam ring via attack of a hydroxide ion on the β -lactam carbonyl carbon, with no formation of covalent adducts (17,35,47-49).

The zinc ion in the first binding site (Zn1 or histidine site) is coordinated by four ligands in a tetrahedral geometry: the nitrogen atom of the imidazole groups of three histidine residues [His86(116), His88(118) and His149(196)] and the oxygen atom of a water molecule or hydroxide ion; this oxygen ligand is a bridge to the second zinc ion. The zinc in the second binding site (Zn2 or cysteine site) is coordinated by five ligands: three other amino acid side chains [Asp90(120), Cys168(221) and His210(263)] in a distorted trigonal bipyramidal geometry, an apical water molecule and the bridging water/hydroxide, which probably acts as the nucleophile in the course of β -lactam hydrolysis (3,17).

Zinc-bound β -lactamases appear to be more stable than their corresponding metal-depleted forms (9) and removal of the metal is known to induce conformational changes (40,46,50). No detailed information on the conformational stability of MBLs has, however, been reported to date (for a brief review of the literature, see the discussion section). In the present work, the chemical-induced unfolding transitions of both apo- and holoBcII were studied by using a combination of spectroscopic techniques. This analysis gives insights into the role of zinc in stability and provides estimates of the thermodynamic parameters. Furthermore, data obtained at moderate denaturant concentrations indicate population of a heterogeneous ensemble of interconverting partially folded species with two zinc ions bound and modest structural changes at the enzyme surface, particularly in the two active site loops. Observation that these species display no significant changes in the geometry of

the active site but are fully inactive demonstrates that both the β 3- β 4 and β 11- α 3 loops are important structural elements for catalysis.

This study brings new insights into the role of metal cofactors in protein folding as a whole, in the absence of any clinical implications. Moreover it highlights structural aspects linked to the catalytic activity of the enzyme, which are relevant to inhibitor discovery.

RESULTS

The fluorescence spectra of holo and apoBcII (Figures 2A,B), measured at pH 7.5, 25°C, are similar and display a broad emission band with maxima at 329 and 334 nm, respectively. These relatively low maximum emission wavelengths (λ_{max}) are consistent with low solvent exposure of the four tryptophan indole side chains, as seen in the enzyme 3D structure (Figure 1). In 4 M GdmCl, λ_{max} is shifted to 355-356 nm (Figures 2A,B), indicating full solvent accessibility of tryptophan indole groups. The near-UV CD spectra (not shown) of free and metal-bound BcII are also similar, although not identical, indicating a well-defined tertiary structure in both cases. The far-UV CD spectra of holo and apoBcII, shown in Figures 2C,D, reveal a significant decrease in helical content of the enzyme in the absence of zinc; this was previously estimated to be around 10 % (46). With both apo- and holoenzyme, addition of high concentrations of denaturant led to a dramatic reduction of the CD signal (Figures 2C,D), consistent with a major decrease in secondary structure organization.

Incubation of both apo- and holoBcII (0.15 mg·mL⁻¹, i.e. 6 μ M) for 12 h in 6 M GdmCl, and subsequent dilution, restored fluorescence and far-UV CD spectra that are indistinguishable from those of the native state, indicating that GdmCl-induced unfolding is fully reversible for both forms of the enzyme. With holoBcII, this could be further demonstrated by measuring full recovery of the enzyme activity after unfolding/refolding cycles. Thus, fluorescence and CD spectroscopy were used to follow unfolding transitions of the enzyme by GdmCl and urea.

Unfolding of apoBcII—With the metal-depleted form of the enzyme, the coincidence of

the transition curves obtained by intrinsic fluorescence and far-UV CD measurements (Figure 2F) indicated that secondary and tertiary structures were destabilized concomitantly. The unfolding curves for the GdmCl-induced denaturation in the absence of zinc can be described by an apparent cooperative two-state model ($N \rightleftharpoons U$), where only the native and unfolded states are significantly populated. Dilution of the fully denatured enzyme (in 6 M GdmCl) into final denaturant concentrations corresponding to the transition zone (i.e. 1-2 M GdmCl) showed that the process was monitored under genuine equilibrium conditions and occurred with full thermodynamic reversibility. Therefore, values of the thermodynamic parameters were calculated assuming a simple two-state model (Table 1). Notably, values obtained for the Gibbs free energy of unfolding (ΔG°_{NU}) were identical, within the error limit, for both optical methods and also for unfolding induced by either GdmCl or urea, providing convincing evidence for a simple two-state unfolding mechanism.

Unfolding of holoBcII—By contrast, in spite of full thermodynamic reversibility, unfolding of holoBcII with both GdmCl (Figure 2E) and urea (data not shown) displayed non-cooperative behaviour, with at least two unfolding transitions. However, since the enzyme was not fully unfolded in 10 M urea (note that no significant unfolding could be observed by both intrinsic fluorescence and far-UV CD measurements at concentrations below 7 M), data obtained using this denaturant were not further analysed.

With GdmCl, the first and second transitions occurred with midpoint values of 1.9 and 2.8 M, respectively. Both were characterized by changes in intrinsic fluorescence and far-UV CD (Figure 2E; also near-UV CD, data not shown). These data indicate population of species with intermediate conformations that are in equilibrium with native and fully unfolded enzyme molecules. Optical measurements at 2.4 M GdmCl, i.e. close to the end of the first apparent transition, suggest the existence of a stable intermediate state that retains both a high content of native secondary structure, as deduced from the far-UV CD spectrum shown in Figure 2C, and a significant protection of the tryptophan residues from the solvent, as indicated by the fluorescence spectrum

shown in Figure 2A. The fluorescence and far-UV CD data shown in Figure 2E were analysed separately on the basis of a three-state model ($N \rightleftharpoons I \rightleftharpoons U$), using equation (3), and the corresponding thermodynamic parameters are given in Table 2. GdmCl-induced unfolding of holoBcII was also followed by activity measurements (Figure 2E), which indicated that the catalytic activity is lost in a single transition, with a midpoint of 1.9 M, concurrent with the first transition observed by optical methods. The possibility of a denaturant ionic strength effect could be excluded by showing that no significant change in enzymatic activity occurred in the presence of NaCl at concentrations up to 3 M (not shown). The intermediate state that is apparently populated for the first unfolding transition is thus totally inactive, suggesting a change in specific tertiary and/or secondary structure organization at the enzyme active site, and possibly zinc release.

Finally, GdmCl-induced unfolding was also performed in the presence of the hydrophobic dye ANS; fluorescence measurements at 475 nm revealed no significant enhancement in intensity, and thus no ANS binding, indicating that no species (such as a molten globule (62)) having significant hydrophobic regions exposed to the solvent is significantly populated (63-65).

Characterization of the intermediate state—Since the intermediate state is enzymatically inactive, one obvious possibility is that the catalytically essential zinc atoms have dissociated from the enzyme. To gain more insight into the presence of zinc during holoBcII unfolding, the imidazole resonances of the histidine residues involved in the coordination of zinc ions (i.e. His86(116), His88(118) and His149(196) of the histidine site, and His210(263) of the cysteine site) were followed as a function of GdmCl concentration. Figure 3A shows ^1H - ^{15}N HSQC spectra focusing on the imidazole signals in the presence (holoBcII) and absence (apoBcII) of zinc, with no GdmCl. The imidazole resonances of the four histidines are well defined and assigned when zinc ions are bound to the catalytic site (51), but not in their absence. The clear difference between holo- and apoBcII in the NMR crosspeak pattern of their imidazole groups allowed detailed analysis of the effect of various GdmCl concentrations on the binding of zinc. At all GdmCl concentrations

between 0 and 2.5 M, imidazole signals of the four binding histidines could be distinctly observed (Figure 3B). Furthermore, the increase of GdmCl concentration from 0 to 2.5 M caused only slight displacements of the imidazole signals (Figure 3B), close to the experimental error, suggesting little change in the geometry of the zinc binding sites. These data unambiguously demonstrate that the two zinc ions are bound to their respective sites throughout the first unfolding transition and therefore, the loss of enzymatic activity is not due to the release of zinc. Furthermore, while there is evidence that the zinc ions have the flexibility to move significantly within the active site (31,66), the very modest shifts of the imidazole crosspeaks of the zinc ligands suggest that addition of 2.5 M GdmCl not only does not lead to the release of the zinc atoms but in fact has very little effect on the structure of their coordination sites.

The dynamic accessibility of the tryptophan residues in folded ($[GdmCl] = 0\text{ M}$), intermediate ($[GdmCl] = 2.4\text{ M}$) and unfolded ($[GdmCl] = 3.5\text{ M}$) states of holoBcII was investigated using acrylamide as a fluorescence quencher (67). As the acrylamide concentration was increased, the fluorescence intensity decreased without a noticeable change in spectral shape and the data were analysed according to equation 1 to determine the quenching constant (K_{sv}) (Figure 4). Complete unfolding of holoBcII in the presence of 3.5 M GdmCl caused a *ca.* 4.5-fold increase of the Stern-Volmer quenching constant, from 1.8 ± 0.1 (in the absence of denaturant) to $8 \pm 0.2\text{ M}^{-1}$, attributable to high solvent exposure of tryptophan side chains in the unfolded protein. By contrast, the Stern-Volmer quenching constant in 2.4 M GdmCl, i.e. $K_{sv} = 1.9 \pm 0.2\text{ M}^{-1}$, is identical to that of the folded state, showing no significant change in the solvent accessibility of the tryptophan residues under these conditions.

To obtain amino-acid specific information on the unfolding mechanism of BcII, a series of 2D ^1H - ^{15}N HSQC NMR spectra was recorded under equilibrium conditions in the presence of various GdmCl concentrations in the range from 0 to 4 M. These experiments were performed at pH 6.5, rather than pH 7.5, in order to slow down intrinsic amide hydrogen exchange. Figure 5 shows representative spectra of ^{15}N -BcII, collected in the presence of 0, 1.63, 2.34 and 4 M GdmCl. In

the absence of denaturant (Figure 5A), the protein spectrum showed a set of well-dispersed peaks characteristic of the folded state (68). At 4 M GdmCl (Figure 5D), all native enzyme signals disappeared and the spectrum is typical of an unfolded protein. At intermediate GdmCl concentrations (e.g. 1.63 and 2.34 M), corresponding to the first unfolding transition (see Figure 2), spectra (Figures 5B,C) were similar to that of the folded state (Figure 5A). Changes in both chemical shift and peak intensity could be observed throughout the entire range of denaturant concentrations. Up to 1.5 M GdmCl, all peaks displayed chemical shifts close to their native state values, although with reduced intensities (probably due to exchange broadening), whereas at higher denaturant concentrations, disappearance of some peaks occurred. At 2.34 M GdmCl, some peaks corresponding to the unfolded state could be observed (Figure 6).

Based on the resonance assignments of native holoBcII (68), assignments of the resonances of the enzyme in the presence of GdmCl concentrations ranging from 0 to 2.34 M could be achieved simply by following chemical shift changes as a function of denaturant concentration. The chemical shifts of 184 out of 227 residues (Figure 7) were monitored in this way and, for most of them, changes occurred progressively and linearly with denaturant concentration. For 6 residues (i.e. Lys134(181), Lys147(194), His149(196), Leu178(231) and also two unassigned ones), non-linear (i.e. curved; see Figure 6) chemical shift changes were observed, however, suggesting that more than two states (i.e. in addition to N and I) are involved.

A detailed analysis of the chemical shift data (Figure 7) showed that 59 residues were significantly perturbed by the denaturant (i.e. $\text{CSP} > 0.064\text{ ppm}$ between 0 and 2.34 M GdmCl). Among these, the signals of 8 residues [Lys50(78), Thr64(92), Glu72(100), Ile83(113), Ala115(146), Thr131(178), Val165(218), Glu188(243)] disappeared completely as GdmCl concentration was increased above 0.75 M, presumably as a result of exchange broadening due to a large shift difference between the native and intermediate states. Those 59 residues, which are all significantly exposed to the solvent (as computed with NACCESS (69)), are represented schematically

on the structure in Figure 7B. 32 of them are located in loop regions, while the remaining 27 residues are found essentially at the ends of well-organized secondary structure elements, i.e. 16 in β -strands and 11 in α -helices (Figure 7B). These 11 residues in α -helices correspond to *ca.* 18 % of the total number of α -helical residues in the enzyme structure, which is in good agreement with the *ca.* 17 % loss in negative ellipticity measured at 222 nm, between 0 and 2.4 M GdmCl (Figures 2C,E). These data suggest that the denaturant induces significant conformational changes in the corresponding regions of the polypeptide backbone. We were able to follow specifically the resonances of 50 residues whose backbone amides are fully buried in the enzyme core (as computed with NACCESS (69)), and we observed that they do not undergo any significant shift perturbation (Table S1), with the exception of Val25(52), Leu63(91), Leu67(95) and Val207(260), which are in fact positioned close to polar residues that experience significant shift changes. Most importantly, HSQC spectra collected in the presence of urea (data not shown) yielded similar results, thus indicating that no ionic strength effect was observed with GdmCl. In the case of residues located around the active site, these results are in good agreement with the observation that addition of 3 M NaCl had no effect on the enzyme activity (see above).

Figure 8 shows CSPs of the amide and indole ^1H - ^{15}N signals of the four tryptophan residues. Progressive and approximately linear shift changes occur with increasing GdmCl concentrations, in good agreement with the behaviour of most of the backbone resonances. The side chain of Trp189(244), which is completely buried in the core of the native protein, showed only minor chemical shift perturbation (0.02 ppm, see Figure 8) in the presence of the denaturant, indicating the high stability of its immediate environment during the first unfolding transition. Accordingly, residues in the vicinity of Trp189(244) remained in a native-like state up to at least 2.4 M GdmCl. By contrast, indole groups of Trp59(87) and Trp157(204) are more exposed to the solvent and their environment proved to be a little more sensitive to the denaturant, as shown by CSPs of 0.08 ppm and 0.06 ppm, respectively, in 2.34 M GdmCl (Figure 8). Finally, Trp26(53) side

chain, which shows very limited solvent accessibility, underwent a dramatic chemical shift perturbation at low GdmCl concentration. Thus, the CSP was 0.14 ppm at 0.5 M GdmCl and the signal totally disappeared at higher concentrations, probably due to exchange broadening. Since the emission fluorescence intensity of the enzyme measured at 370 nm does not change significantly in the presence of GdmCl concentrations lower than 1.5 M (Figure 2E), these results suggest that Trp59(87) and/or Trp157(204), and not Trp26(53) are responsible for the increase in intensity observed at higher concentrations (Figures 2A,E). For all four tryptophan residues, however, up to 2 M GdmCl the backbone resonance CSP (Figure 2B) remained below the computed threshold for significant CSP (CSP > 0.064 ppm), in good agreement with the view that the enzyme hydrophobic core remains largely unaffected.

Refolding of apoBcII by the addition of zinc ions—Transition curves for apo and holoBcII (Figures 2E and 2F, respectively) highlight significant differences in their conformational stabilities (see also Tables 1 and 2). Thus, at *ca.* 2 M GdmCl, whereas apoBcII is completely unfolded, its dizinc counterpart adopts a native-like, although catalytically inactive, conformation. Using ^1H - ^{15}N HSQC experiments for selective observation of His imidazole, as described above, we monitored refolding of BcII unfolded in 2 M GdmCl in the absence of zinc, upon addition of one and two molar equivalents of zinc (Figure 9). In the presence of denaturant, addition of zinc caused changes in the spectrum of the enzyme, with the concomitant appearance of narrow peaks corresponding to histidine imidazole signals of native holoBcII, and disappearance of the broad peaks characteristic of the histidine imidazole signals of the unfolded protein. At a Zn/BcII molar ratio of 1, the histidine imidazole ^1H - ^{15}N HSQC spectrum (Figure 9C) showed a peak distribution consistent with significant population of both unfolded and dizinc-bound BcII. The absence of any signal for a putative monozinc form indicates cooperative binding of the two metal ions (46). Finally, in the presence of two equivalents of zinc (i.e. Zn/BcII molar ratio of 2), complete recovery of a spectrum (Figure 9D) characteristic of native BcII is observed. These results demonstrate that even in the presence of 2 M GdmCl, zinc binds

cooperatively to the enzyme and hence shifts the reversible denaturation by GdmCl from an unfolded state to a native-like intermediate state.

DISCUSSION

As reported before (46,51,70), the metal-depleted form of the enzyme is catalytically inactive and displays significant changes in its spectroscopic properties, suggesting both a catalytic and structural role for the metal ions in BcII β -lactamase. The conformational properties of both metal-free and dizinc forms of BcII β -lactamase were probed using chemical denaturants. Full reversibility of the unfolding process was established by both spectroscopic methods (i.e. fluorescence, CD and NMR) and enzymatic assays. In particular, imidazole-optimized HSQC experiments (Figure 9) showed that zinc binding to the apoenzyme unfolded in the presence of 2 M GdmCl shifts the equilibrium to the intermediate partially folded state.

Equilibrium folding experiments showed major destabilization of the enzyme in the absence of zinc. Thus, although unfolding of BcII proved to be fully reversible in both the absence and presence of zinc (Figures 2 and 9), transition curves obtained by measuring fluorescence and CD (Figures 2E,F) showed clear differences. While unfolding of apoBcII starts at 1 M GdmCl and follows a simple two-state cooperative transition ($N \rightleftharpoons U$), with $C_m = 1.5$ M (i.e. transition midpoint), the metal-bound β -lactamase remains fully active in the presence of 1.5 M GdmCl and, at higher denaturant concentrations, unfolds non-cooperatively in an apparent three-state transition ($N \rightleftharpoons I \rightleftharpoons U$), with C_m values of *ca.* 1.9 and 2.8 M. These data are consistent with heat-induced denaturation of the enzyme (71). Thus, unfolding of the metal-bound species was best described by a three-state model, with apparent T_m values of 72 ± 2 and $85 \pm 3^\circ\text{C}$ (71), whereas the apoenzyme was found to unfold in a two-state transition, with apparent $T_m = 62.3 \pm 0.02^\circ\text{C}$ (71). Thermal unfolding of both enzyme forms proved irreversible, however, and thus no further quantitative analysis could be performed.

Analysis of apo- and holoBcII chemical-induced unfolding curves was performed on the

basis of two- and three-state models, respectively, and fitting the corresponding equations to the data in Figures 2E,F yielded values of the thermodynamic parameters displayed in Tables 1 and 2. With both forms, transition curves obtained by intrinsic fluorescence and far-UV CD measurements (also near-UV CD, not shown) indicated that secondary and tertiary structures are destabilized simultaneously, albeit in one and two transitions in the absence and presence of zinc, respectively. This analysis suggests that in the presence of zinc, a partially folded state with reduced fluorescence and CD signal intensities is maximally populated at *ca.* 2.4 M GdmCl. The coincident loss in both signals at all denaturant concentrations, combined with the absence of ANS binding, discards the possibility of a molten globule intermediate (62-65).

For apoBcII, the Gibbs free energy of unfolding ($\Delta G^\circ_{\text{NU}}$) was calculated to be 32 ± 2 $\text{kJ}\cdot\text{mol}^{-1}$ (Table 1) and the corresponding m_{UN} ($= -m_{\text{NU}}$) values are 20 ± 1 and 9.9 ± 0.2 $\text{kJ}\cdot\text{mol}^{-1}\cdot\text{M}^{-1}$ for GdmCl and urea, respectively. Interestingly, the experimental m_{UN} values are 10-20% smaller than predicted from the expected change in solvent accessible surface area upon folding (22.2 and 13 $\text{kJ}\cdot\text{mol}^{-1}\cdot\text{M}^{-1}$ in GdmCl and urea, respectively; estimated from the size of the enzyme (72)), a finding consistent with an increase of the protein surface exposed to solvent in native apoBcII. On the basis of a three-state model, values of the thermodynamic parameters (i.e. $\Delta G^\circ_{\text{NU}}$ and m_{UN}) for holoBcII were found to be 80-95 $\text{kJ}\cdot\text{mol}^{-1}$ and 30-40 $\text{kJ}\cdot\text{mol}^{-1}\cdot\text{M}^{-1}$, respectively (Table 2). Whereas for the second structural transition, fluorescence and CD measurements yielded values that are identical within the error limit (Table 2), major differences between these two measurements appeared for the first transition. In both cases, the global $\Delta G^\circ_{\text{UN}}$ value (≥ 80 $\text{kJ}\cdot\text{mol}^{-1}$) is significantly greater than the 20-60 $\text{kJ}\cdot\text{mol}^{-1}$ found in textbooks (see e.g. (73-76)) for most proteins. Furthermore, the corresponding experimental m_{UN} value (≥ 30 $\text{kJ}\cdot\text{mol}^{-1}$ in GdmCl) is also well above that calculated from the size of the protein (22.2 $\text{kJ}\cdot\text{mol}^{-1}$ (72)). Thus, values of the thermodynamic parameters in Table 2 suggest that a three-state model might be too simple a description of holoBcII unfolding. This is further supported by the observation that a number of

residues, notably Leu178(231) in the β 11- α 4 loop, show a non-linear dependence of their amide chemical shifts on GdmCl concentration in the range 1.0 – 2.34 M (Figure 6), indicating the presence of more than two states in this concentration range.

Aiming at a better description of the unfolding mechanism of BcII metallo- β -lactamase, we analysed in detail the structural features of the intermediate state that apparently forms in a non-cooperative manner at moderate GdmCl concentration (Figures 2A,C,E). While the enzyme was found to lose its activity in the 1.5-2.5 M GdmCl concentration range, optical methods indicated population of a partially folded state, which is not a molten globule and which displays a high content of structural organization, at both the secondary and the tertiary levels. Thus, far-UV CD measurements indicated that the protein retains *ca.* 83 % of its α -helical content in the presence of 2.4 M GdmCl and both fluorescence quenching and ANS binding experiments suggested conservation of a compact and well-organized protein core. 2D NMR experiments allowed the effect of both GdmCl and urea to be monitored at the level of individual residues. In particular, long-range ^1H - ^{15}N HSQC for selective observation of His imidazole resonances demonstrated that the loss of catalytic activity, concomitant with the first transition observed by optical methods, is not due to the loss of zinc from the enzyme active site, which in fact remains occupied by both metal ions up to 2.5 M GdmCl, with no significant change in its geometry. Classical ^1H - ^{15}N HSQC experiments were performed in the presence of GdmCl and urea to probe the effect on the environment of 184 and 181 residues, respectively, out of 227 in the full-length protein. In the GdmCl and urea concentration ranges of 0 to 2.34 M and 0 to 7.9 M, respectively, 2D NMR data showed progressive changes of the chemical shift of many residues, with significant (CSP > 0.064 ppm and CSP > 0.079 ppm, respectively) perturbations for 59 and 40 residues, respectively. These data suggest a gradual transition from the native state to intermediate states with only modest structural changes as indicated by the NMR spectra. These changes are seen to occur at the surface of the enzyme structure and are well localized in loop structures, and at the N- and C-terminal

extremities of α -helices and β -strands. HSQC experiments thus confirm population of globular species, with a well-organized, compact, solvent-protected hydrophobic core. Upon increasing GdmCl concentration in the range of 1.5 to 2.5 M, the equilibrium between these interconverting folding intermediates is shifted towards the less structured one, characterized by a reduction of *ca.* 17 % and *ca.* 25 % in CD (at 222 nm) and fluorescence (at 370 nm) intensity, respectively. Thus, all the data are consistent with the first transition leading to the non-cooperative formation of a heterogeneous ensemble of native-like protein molecules, with two zinc ions bound in the active site but no catalytic activity. A single distinct folding intermediate (e.g. molten globule) is not formed and a simple three-state model cannot be used to fit the data. In contrast, the second transition from these multiple interconverting native-like species to the fully unfolded state seems to occur with full cooperativity. Interestingly, the corresponding *m* value ($m_{\text{IN}} = 23.5 \pm 0.7 \text{ kJ}\cdot\text{mol}^{-1}\cdot\text{M}^{-1}$) is about the same than that calculated for the native enzyme ($m_{\text{UN}} = 22.2 \text{ kJ}\cdot\text{mol}^{-1}\cdot\text{M}^{-1}$ (72)), suggesting that the surface that is not accessible to the solvent becomes entirely exposed in this transition. This observation strengthens the conclusion that the first transition leads to the formation of native-like, zinc-bound species, with no significant opening of the protein structure and only limited, superficial, conformational changes. These are sufficient, however, to cause complete enzyme inactivation.

Finally, our results reveal that global unfolding of the protein takes place over a narrow GdmCl concentration range of 2.5 to 3.0 M, in a cooperative transition characterized by a Gibbs free energy change (ΔG°) of $65 \pm 1.4 \text{ kJ}\cdot\text{mol}^{-1}$ and a corresponding *m* value of $23.5 \pm 0.7 \text{ kJ}\cdot\text{mol}^{-1}\cdot\text{M}^{-1}$. These values are compatible with unfolding of the enzyme occurring in a single cooperative transition, from native-like intermediate species to the fully unfolded state. Although holoBcII β -lactamase is remarkably stable, removal of zinc, however, causes a dramatic destabilization of *ca.* $35 \text{ kJ}\cdot\text{mol}^{-1}$. This finding is consistent with current knowledge that metal cofactors often stabilize the native state of the bound protein (77,78). The effect of zinc on the stability of three other MBLs was studied in some

details. With subclass B1 BlaB and VIM-4 β -lactamases, zinc ions were observed to stabilize the enzyme. GdmCl unfolding of BlaB (79) monitored by intrinsic fluorescence measurements occurred at significantly lower denaturant concentration for the apoform than for the two zinc-bound species. Although the data were interpreted on the basis of a three-state model, the lack of reversibility observed in experiments measuring the restoration of catalytic activity seriously compromises any quantitative analysis. With VIM-4 (80) a dramatic decrease in thermal stability (i.e. a drop of 27°C in the apparent T_m value) was observed in the absence of zinc. Likewise, with CphA β -lactamase (36), a subclass B2 carbapenamase which is active in the monozinc form only, the catalytic zinc was found to increase the thermal stability by *ca.* 14°C, whereas the dizinc inactive form was found to be even more resistant to temperature (i.e. a further increase of 4°C in T_m) than the monozinc enzyme. Finally, study of human glyoxalase II (81), another enzyme of the MBL superfamily, suggested that chemically-induced unfolding is a multistep process. Very low GdmCl concentrations (< 1 M) were seen to inactivate the enzyme, with no release of zinc and no significant optical changes (both intrinsic fluorescence and CD), an observation which is reminiscent of what is found in the present work. Further increase in denaturant concentration led, however, to the formation of a molten globule (with apparent maximum population at 1.2 M (81)), before leading to complete unfolding at concentrations above 3 M.

All the results in this work point at the major structural role of zinc. Up to *ca.* 2.5 M GdmCl, the presence of zinc in the active site appears to lock the protein in an ensemble of native-like structures. The NMR experiments, however, show that there are definite, though limited, structural changes at the enzyme surface, at this GdmCl concentration. These limited surface changes must give rise to the observed loss of catalytic activity. In particular, substantial CSPs are seen to occur in the β 3- β 4 [residues 32-38(59-66)] and β 11- α 4 [170-188(223-241)] loops that flank the enzyme active site, and also for Asp90(120) in the Zn²⁺ site. It is notable that all these residues also show substantial CSPs on the binding of an inhibitor to the active site (31). The

large CSP observed for Asp90(120) in this work (Figure 7) most likely results from changes in its environment and not in its position, since observation of imidazole chemical shifts demonstrated that the geometry of both Zn binding sites remains largely unaffected by GdmCl concentrations below 2.5 M. As for the loops, both have been well documented to be flexible and to modulate, by conformational changes, the shape of the active site (see references below). The NMR solution structure (31) showed that, despite significant flexibility, both structural elements display a relatively well-defined conformation. They are generally considered to play a critical role for catalytic activity, especially in the ability of MBLs to hydrolyse β -lactam antibiotics of very diverse structures (for recent detailed reviews, see (11,17)). In particular, the β 3- β 4 loop [32-38(59-66)] (also known as the “mobile loop” or “flap”), which is conserved in most class B1 MBLs, has been shown to move towards bound inhibitors and substrates, and thus to contribute to the formation of a hydrophobic pocket which is important for ligand binding (see e.g. (31,40,82-100)). Together with the “flap”, the β 11- α 4 loop [170-188(223-241)] on the other side of the active site also contributes to the capacity of MBLs to bind a structurally broad range of substrates and inhibitors (87,89,90,100). In particular, recent crystal structures of NDM-1 MBL (100,101) have provided further evidence that residues Lys(224) and Asn(233) (BBL numbering; these two residues are conserved in BcII, IMP-1 and CCrA; His(224) and Tyr(224)/Arg(228) are found in VIM-1 and VIM-2, respectively) in the β 11- α 4 loop play a direct role in substrate binding and hydrolysis. A combination of structural and computational studies of NDM-1 (66) has led to the suggestion that movements of the two loops are important not only in substrate binding but also in the hydration of the active site, including the water molecules which play a central role in the catalytic mechanism. Observation in this work that relatively modest structural changes in the partially folded species, particularly in the two active site loops, lead to complete loss of catalytic activity provides further evidence that these structural elements are key determinants of the enzyme catalytic activity and thus are relevant to the discovery of effective inhibitors.

EXPERIMENTAL PROCEDURES

Enzyme and Chemicals—Ultrapure guanidinium chloride (GdmCl) and benzylpenicillin were purchased from Sigma-Aldrich. All other chemicals were of reagent grade.

Both the recombinant (46) and uniformly ^{15}N isotopically enriched (51) β -Lactamase II from *Bacillus cereus* 569/H/9 (BcII) were expressed and purified as described. The enzyme concentration was determined by absorbance measurements at 280 nm, using a molar extinction coefficient value of $30500 \text{ M}^{-1}\cdot\text{cm}^{-1}$ (43).

The metal-free BcII enzyme (apoBcII) was prepared following the procedure described in Jacquin *et al.* (46). All final preparations were stored at -20°C .

Buffers—Unless otherwise mentioned, experiments were performed in 10 mM Hepes buffer, pH 7.5, with 300 mM NaCl in the presence (holoBcII) or absence (apoBcII) of 0.1 mM ZnSO_4 . GdmCl and acrylamide solutions were prepared in the same buffer, and, if necessary, pH was adjusted to 7.5 with HCl or NaOH.

Enzyme Activity Measurements—Hydrolysis of benzylpenicillin was monitored by measuring absorbance changes at 235 nm using a Specord 200 spectrophotometer (Analytik Jena) equipped with a thermostatically controlled cell holder. Values of the kinetic parameters were determined at 30°C in 10 mM Hepes, pH 7.5, as described (52).

Chemical-Induced Unfolding Transitions—Unfolding was studied at 25°C . Samples at various denaturant (GdmCl and urea) concentrations were allowed to equilibrate for at least 12 h (under these conditions, equilibrium is reached throughout the transition, see results). Unfolding and refolding transitions were obtained by monitoring the changes in intrinsic fluorescence emission ($\lambda_{\text{exc}} = 280 \text{ nm}$; $\lambda_{\text{em}} = 370 \text{ nm}$) and circular dichroism (CD) at 222 nm, using a Varian Cary Eclipse spectrofluorimeter and a Jasco J-810 spectropolarimeter, respectively, both equipped with a thermostatically controlled cell holder. With all samples, the data were corrected for the contribution of the solution (buffer + denaturant). Unfolding of holoBcII was also monitored by

measuring enzyme activity, as described above. Denaturant concentrations in the samples were determined from refractive index measurements (53) using a R5000 hand-held refractometer from Atago (Japan). Protein concentrations of *ca.* $0.15 \text{ mg}\cdot\text{mL}^{-1}$ ($6.0 \mu\text{M}$) were used throughout.

Quenching of Tryptophan Fluorescence by Acrylamide—All fluorescence experiments were performed at 25°C using a protein concentration of $0.10 \text{ mg}\cdot\text{mL}^{-1}$ ($4 \mu\text{M}$). The enzyme was diluted with acrylamide concentrations ranging from 0 to 0.2 M and tryptophan fluorescence emission spectra were recorded from 305 to 450 nm, following excitation at 295 nm. Each spectrum was the average of five acquisitions and was corrected for the contribution of the solution. The solvent accessibility of tryptophan residues was estimated according to the Stern-Volmer equation (54):

$$\frac{F_0}{F} = 1 + K_{sv}[Q] \quad \text{Equation 1}$$

where F_0 and F are the tryptophan fluorescence intensities (computed as areas below the curves for the tryptophan emission fluorescence spectra) in the absence and presence of acrylamide, respectively, K_{sv} is the Stern-Volmer quenching constant and $[Q]$ is the molar concentration of acrylamide.

Nuclear Magnetic Resonance (NMR)—Freeze-dried ^{15}N labelled holoBcII was dissolved in 10 mM Hepes buffer (pH 6.5), containing 300 mM NaCl and 0.1 mM ZnSO_4 , to give a final enzyme concentration of $10 \text{ mg}\cdot\text{mL}^{-1}$ ($400 \mu\text{M}$) in the presence of GdmCl or urea concentrations ranging from 0 to 4 M or 0 to 7.9 M, respectively. NMR spectra were collected using a home-built 750 MHz NMR spectrometer, controlled with GE/Omega software and equipped with an Oxford Instruments Co. magnet and a home-built triple-resonance pulse-field-gradient probe head. Spectral widths of 10204.08 Hz and 2659.57 Hz in $F2$ (^1H) and $F1$ (^{15}N) respectively, were used for 2D ^1H - ^{15}N HSQC spectra. All spectra were collected at 25°C , processed with NMRPipe (55) and analysed with CcpNmr Analysis (56).

For chemical-induced unfolding under equilibrium conditions, the concomitant population of folded and unfolded species in the transition

region is accompanied by changes in the NMR spectrum, both in terms of peak intensity and chemical shifts. The combined chemical shift perturbation (CSP) was calculated as follows (57):

$$CSP = \sqrt{[(\Delta\delta^1H)^2 + (0.15 \times \Delta\delta^{15N})^2]}$$

Equation 2

where δ represents the chemical shift in ppm.

In order to determine significant shift changes, we defined a threshold value, as follows. In a first step, all shift distances were considered and averaged ($\langle CSP \rangle$), with errors calculated at the 95 % confidence limit (i.e. twice the standard deviation, σ). Then, the highest shift changes ($CSP \geq \langle CSP \rangle + 2\sigma$) were removed from the data and a new $\langle CSP \rangle$, with standard deviation, was calculated. This operation was repeated until all data lie within 2 sigma values of the average. And the final $\langle CSP \rangle + 2\sigma$ value corresponds to the threshold below which the residues are not significantly perturbed.

The 2D 1H - ^{15}N HSQC experiments for the observation of histidine imidazole groups were carried out with a total dephasing delay of 16.67 ms, at 25°C, on a Bruker Avance 600 MHz NMR spectrometer equipped with a cryoprobe. The apoprotein concentration was 12.5 mg·mL⁻¹ (500 μ M) in 10 mM HEPES, 300 mM NaCl, pH 7.5. One and two molar equivalents of zinc ions were added to the same sample.

Data Analysis—Unfolding curves were analysed on the basis of a two-state (N \rightleftharpoons U) or a three-state (N \rightleftharpoons I \rightleftharpoons U) model, according to Vandenameele *et al.* (58) and equation 3, respectively. This analysis is based on the assumption that the differences in Gibbs free

energy between various species exhibit a linear dependence on denaturant concentration (59,60):

$$y_{obs} = \frac{[y_N + \exp(a)y_I + \exp(a)\exp(b)y_U]}{[1 + \exp(a) + \exp(a)\exp(b)]}$$

Equation 3

with

$$a = -\frac{[\Delta G^\circ(H_2O)_{N-I} + m_{N-I}[GdmCl]]}{RT} \quad \text{and}$$

$$b = -\frac{[\Delta G^\circ(H_2O)_{I-U} + m_{I-U}[GdmCl]]}{RT}$$

y_{obs} is the measured parameter at a given denaturant concentration, and y_N , y_I and y_U are the values of this parameter for the folded, partially unfolded (intermediate) and unfolded states, respectively, at the same denaturant concentration. The observed linear dependence of this parameter on denaturant concentration was taken into account as described (61). $\Delta G^\circ(H_2O)_{N-I}$ and $\Delta G^\circ(H_2O)_{I-U}$ represent the unfolding free energy on going from N to I, and I to U, respectively, in the absence of denaturant; m_{N-I} and m_{I-U} are the slopes, $\delta(\Delta G^\circ)/\delta[GdmCl]$, of the corresponding linear plots of the Gibbs free energy against denaturant concentration. R is the gas constant, and T is the absolute temperature. The midpoints of the transition, i.e., the denaturant concentrations at which $[I]/[N]$ and $[U]/[I]$ are equal to unity, are given by $C_m = -\Delta G^\circ(H_2O)/m$

The program Graft 5.0.10 (Erithacus Software Ltd.) was used for non-linear least-squares analysis of the data. Unless otherwise stated, errors are reported as standard deviations throughout.

Acknowledgements: The authors acknowledge Prof. Jean-Marie Frère for critical reading of the manuscript and Prof. Roger H. Pain for his suggestion of a ‘punchy’ title. Also we are grateful to Dr. Catherine Goodman (acting on behalf of the Journal of Biological Chemistry) for valuable suggestions to improve the manuscript.

Conflict of interest: The authors declare that they have no conflicts of interest with the contents of this article.

Author contributions: C.M. and M.N. contributed equally to this work. AM conceived and coordinated the study and wrote the paper. CM and MN contributed substantially to conception and design, acquisition and analysis of data, and also to writing the article. OJ, NW, MD, AIK contributed significantly to acquisition of data. GCKR, CD, CR contributed decidedly to design, analysis and interpretation of NMR experiments, and also drafting the article. All authors reviewed the results and approved the final version of the manuscript.

REFERENCES

1. Waley, S.G. β -Lactamase: Mechanism of Action. In *The Chemistry of β -Lactams*; Page, M.I., Ed.; Blackie, London, UK, 1992; pp 198-228.
2. Frère, J.M. β -Lactamases and Bacterial Resistance to Antibiotics. *Mol. Microbiol.* **1995**, *16*, 385-395.
3. Fink, A.L.; Page, M.I. The Mechanisms of Catalysis by β -Lactamases. In *β -Lactamases*; Frère, J.M. Ed; Nova Science Publishers, Inc., New York, 2012; pp. 41-77.
4. Poole, K. Resistance to β -Lactam Antibiotics. *Cell. Mol. Life. Sci.* **2004**, *61*, 2200-2223.
5. Jacoby, G.A.; Munoz-Price, L.S. The New β -Lactamases. *N. Engl. J. Med.* **2005**, *352*, 380-391.
6. Rossolini, G.M.; Docquier, J.D. New β -Lactamases : a Paradigm for the Rapid Response of Bacterial Evolution in Clinical Setting. *Future Microbiol.* **2006**, *1*, 295-308.
7. Frère, J.M., ed. β -Lactamases, Nova Science Publishers, Inc., New York, 2012.
8. Matagne, A.; Dubus, A.; Galleni, M.; and Frère, J.M. The β -Lactamase Cycle: a Tale of Selective Pressure and Bacterial Ingenuity. *Nat. Prod. Rep.* **1999**, *16*, 1-19.
9. Heinz, U.; Adolph, H.W. Metallo- β -lactamases: two Binding Sites for one Catalytic Metal Ion? *Cell. Mol. Life Sci.* **2004**, *61*, 2827-2839.
10. Bebrone, C. Metallo- β -lactamases (Classification, Activity, Genetic Organization, Structure, Zinc Coordination) and their Superfamily. *Biochem. Pharmacol.* **2007**, *74*, 1686-1701.
11. Palzkill, T. Metallo- β -lactamase Structure and Function. *Ann. N.Y. Acad. Sci.* **2013**, *1277*, 91-104.
12. Neuwald, A.F.; Liu, J.S.; Lipman, D.J.; Lawrence, C.E. Extracting Protein Alignment Models from the Sequence Database. *Nucleic Acids Res.* **1997**, *25*, 1665-1677.
13. Daiyasu, H.; Osaka, K.; Ishino, Y., Toh, H. Expansion of the Zinc Metallo-hydrolase Family of the β -Lactamase Fold. *FEBS Lett.* **2001**, *503*, 1-6.
14. Herzberg, O.; Fitzgerald, M.D. Metallo- β -lactamases. In *Handbook of Metalloproteins*; Messerschmidt, A., Bode, W., Gygler, M. Eds.; John Wiley & Sons, Ltd., 2004; Vol. 3, pp 217-234.
15. Bebrone, C.; Garau, G.; Garcia-Saez, I.; Chantalat, L.; Carfi, A.; Dideberg, O. X-ray Structures and Mechanisms of metallo- β -lactamases. In *β -Lactamases*, Frère, J.M., Ed.; Nova Science Publishers, Inc., New York. 2012; pp. 41-77.
16. Baier, F.; Tokuriki, N. Connectivity Between Catalytic Landscapes of the Metallo- β -lactamase Superfamily. *J. Mol. Biol.* **2014**, *426*, 2442-2456.
17. Karsisiotis, A.I.; Damblon, C.F.; Roberts, G.C.K. A Variety of Roles for Versatile Zinc in Metallo- β -lactamases. *Metallomics* **2014**, *6*, 1181-1197.
18. Walsh, T.R.; Toleman, M.A.; Poirel, L.; Nordmann, P. Metallo- β -lactamases: the Quiet Before the Storm? *Clin. Microbiol. Rev.* **2005**, *18*, 306-325
19. Cornaglia, G.; Giamarellou, H.; Rossolini, G.M. Metallo- β -lactamases: a Last Frontier for β -Lactams? *Lancet Infect. Dis.* **2011**, *11*, 381-393.
20. Felici, A.; Amicosante, G.; Oratore, A.; Strom, R.; Ledent, P.; Joris, B.; Fanuel, L.; Frère, J.M. An Overview of the Kinetic Parameters of class B β -Lactamases. *Biochem J.* **1993**, *291*, 151-155.
21. Rasmussen, B.A.; Bush, K. Carbapenem-Hydrolyzing β -Lactamases. *Antimicrob. Agents Chemother.* **1997**, *41*, 223-232.

22. Spencer, J.; Walsh, T.R. A New Approach to the Inhibition of Metallo- β -lactamases. *Angew. Chem. Int. Ed. Engl.* **2006**, *45*, 1022-1026.
23. Drawz, S.M.; Bonomo, R.A. Three Decades of β -Lactamase Inhibitors. *Clin. Microbiol. Rev.* **2010**, *23*, 160-201.
24. Payne, D.J. Metallo- β -lactamases: a New Therapeutic Challenge. *J. Med. Microbiol.* **1993**, *39*, 93-99.
25. Livermore, D.M.; Woodford, N. Carbapenemases: a Problem in Waiting? *Curr. Opin. Microbiol.* **2000**, *3*, 489-495.
26. Oelschlaeger, P.; Ai, N.; DuPrez, K.T.; Welsh, W.J.; Toney, J.H. Evolving Carbapenemases: Can Medicinal Chemists Advance One Step Ahead Of The Coming Storm? *J. Med. Chem.* **2010**, *53*, 3013-3027.
27. Patel, G.; Bobomo, R.A. "Stormy Waters Ahead": Global Emergence of Carbapenemases. *Front. Microbiol.* **2013**, *4*, 48.
28. Bush, K. Proliferation and Significance of Clinically Relevant β -Lactamases. *Ann. N.Y. Acad. Sci.* **2013**, *1277*, 84-90.
29. Fast, W.; Sutton, L.D. Metallo- β -lactamase : Inhibitors and Reporter Substrates. *Biochim. Biophys. Acta* **2013**, *1834*, 1648-1659.
30. Crowder, M.W.; Spencer, J.; Vila, A.J. Metallo- β -lactamases: Novel Weaponry for Antibiotic Resistance in Bacteria. *Acc. Chem. Res.* **2006**, *39*, 721-728.
31. Karsisiotis, A.I.; Damblon, C.F.; Roberts, G.C.K. Solution Structures of the *Bacillus cereus* Metallo- β -lactamase BcII and its Complex with the Broad Spectrum Inhibitor R-Thiomandelic Acid. *Biochem. J.* **2013**, *456*, 397-407.
32. King, A.M.; Reid-YU, S.A.; Wang, W.; King, D.T.; De Pascale, G.; Strynadka, N.C.; Walsh, T.R.; Coombes, B.K.; Wright, G.D. Aspergillomarasmine A Overcomes Metallo- β -lactamase Antibiotic Resistance. *Nature* **2014**, *510*, 503-506.
33. Galleni, M.; Lamotte-Brasseur, J.; Rossolini, G.M.; Spencer, J.; Dideberg, O.; Frère, J.M. Metallo- β -lactamases Working Group Standard Numbering Scheme for Class B β -Lactamases. *Antimicrob. Agents Chemother.* **2001**, *45*, 660-663.
34. Frère, J.M.; Galleni, M.; Bush, K.; Dideberg, O. Is it Necessary to Change the Classification of β -Lactamases? *J. Antimicrob. Chemother.* **2005**, *55*, 1051-1053.
35. Page, M.I.; Badarau, A. The Mechanisms of Catalysis by Metallo- β -lactamases. *Bioinorg. Chem. Appl.* **2008**, *2008*, 14 pages.
36. Hernandez-Valladares, M. ; Felici, A. ; Weber, G. ; Adolph, H. W. ; Zeppezauer, M. ; Rossolini, G. M. ; Amicosante, G. ; Frère, J.M. ; Galleni, M. Zn(II) Dependence of the *Aeromonas hydrophila* AE036 Metallo- β -lactamase Activity and Stability. *Biochemistry* **1997**, *36*, 11534-11541.
37. Sabath, L.D.; Abraham, E.P. Zinc as a Cofactor for Cephalosporinase from *Bacillus cereus* 569. *Biochem. J.* **1966**, *98*, 11C-13C.
38. Meini, M.R.; Llarrull, L.I.; Vila, A.J. Evolution of Metallo- β -lactamases: Trends Revealed by Natural Diversity and *in vitro* Evolution, *Antibiotics* (Basel). **2014**, *3*, 285-316.
39. Carfi, A.; Pares, S.; Duee, E.; Galleni, M.; Duez, C.; Frère, J.M.; and Dideberg, O. The 3-D Structure of a Zinc Metallo- β -lactamase from *Bacillus Cereus* Reveals a New-Type of Protein Fold. *EMBO J.* **1995**, *14*, 4914-4921.

40. Carfi, A.; Duée, E.; Galleni, M.; Frère, J.M.; and Dideberg, O. 1.85 Å Resolution Structure of Zinc β -Lactamase from *Bacillus cereus*. *Acta Crystallogr. D* **1998**, *54*, 313-323.
41. Fabiane, S.M.; Sohi, M.K.; Wan, T.; Payne, D.J.; Bateson, J.H.; Mitchell, T.; Sutton, B.J. Crystal Structure of the Zinc-dependent β -Lactamase from *Bacillus cereus* at 1.9 Å Resolution: Binuclear Active Site with Features of a Mononuclear Enzyme. *Biochemistry* **1998**, *37*, 12404-12411.
42. Garau G.; Garcia-Saez I.; Bebrone C.; Anne C.; Mercuri P.; Galleni M.; Frère J.M.; Dideberg O. Update of the Standard Numbering Scheme for Class B β -Lactamases. *Antimicrob. Agents Chemother.* **1994**, *48*, 2347-2349.
43. Paul-Soto, R.; Bauer, R.; Frère, J.M.; Galleni, M.; Meyer-Klaucke, W.; Nolting, H.; Rossolini, G.M.; de Seny, D.; Hernandez-Valladares, M.; Zeppezauer, M.; Adolph, H.W. Mono and Binuclear Zn^{2+} - β -lactamase. Role of the Conserved Cysteine in the Catalytic Mechanism. *J. Biol. Chem.* **1999**, *274*, 13242–13249.
44. Wommer, S.; Rival, S.; Heinz, U.; Galleni, M.; Frère, J.M.; Franceschini, N.; Amicosante, G.; Rasmussen, B.; Bauer, R.; Adolph, H.W. Substrate-activated Zinc Binding of Metallo- β -lactamases – Physiological Importance of the Mononuclear Enzymes. *J. Biol. Chem.* **2002**, *277*, 24142-24147.
45. Rasia, R.M.; Vila, A.J. Exploring the Role and the Binding Affinity of a Second Zinc Equivalent in *B. cereus* Metallo- β -lactamase. *Biochemistry* **2002**, *41*, 1853-1860.
46. Jacquin, O.; Balbeur, D.; Damblon, C.; Marchot, P.; De Pauw, E.; Roberts, G.C.K.; Frere, J.M.; Matagne, A. Positively Cooperative Binding of Zinc Ions to *Bacillus cereus* 569/H/9 β -Lactamase II Suggests that the Binuclear Enzyme is the Only Relevant Form for Catalysis. *J. Mol. Biol.* **2009**, *392*, 1278-1291.
47. Wang, Z.; Fast, W.; Benkovic, S.J. On the Mechanism of the Metallo- β -lactamase from *Bacteroides fragilis*. *Biochemistry* **1999**, *38*, 10013-10023.
48. Wang, Z.; Fast, W.; Valentine, A.M.; Benkovic, S.J. Metallo- β -lactamase: Structure and Mechanism. *Curr. Opin. Chem. Biol.* **1999**, *3*, 614-622.
49. Frère, J.M. Kinetics of β -Lactamases in Theory and in Practice. In *β -Lactamases*; Frère, J.M., Ed.; Nova Science Publishers, Inc., New York, 2012; pp. 41-77.
50. Hemmingsen, L.; Damblon, C.; Antony, J.; Jensen, M.; Adolph, H.W.; Wommer, S.; Roberts, G.C.K.; Bauer, R. Dynamics of Mononuclear Cadmium β -lactamase Revealed by the Combination of NMR and PAC Spectroscopy. *J. Am. Chem. Soc.* **2001**, *123*, 10329-10335.
51. Damblon, C.; Prosperi, C.; Lian, L. Y.; Barsukov, I.; Paul-Soto, R.; Galleni, M.; Frère, J.M.; Roberts, G.C.K. 1H – 15N HMQC for the Identification of Metal-bound Histidines in ^{113}Cd Substituted *Bacillus cereus* Zinc β -Lactamase. *J. Am. Chem. Soc.* **1999**, *121*, 11575-11576.
52. Matagne, A.; Misselyn-Bauduin, A.M.; Joris, B.; Erpicum, T.; Granier, B.; Frère, J.M. The Diversity of the Catalytic Properties of class A β -lactamases. *Biochem J.* **1990**, *265*, 131-146.
53. Nozaki, Y. The Preparation of Guanidine Hydrochloride. *Method Enzymol.* **1972**, *26*, 43-50.
54. Lakowicz, J.R. Principles of Fluorescence Spectroscopy, 2nd edition, Kluwert Academic/Plenum Publishers, New York, 1999.
55. Delaglio, F.; Grzesiek, S.; Vuister, G.W.; Zhu, G.; Pfeifer, J.; Bax, A. NMRPipe: a Multidimensional Spectral Processing System Based on UNIX pipes. *J. Biomol. NMR.* **1999**, *6*, 277-293.

56. Vranken, W.F.; Boucher, W.; Stevens, T.J.; Fogh, R.H.; Pajon, A.; Llinas, M.; Ulrich, E.L.; Markley, J.L.; Ionides, J.; Laue, E.D. The CCPN Data Model for NMR Spectroscopy: Development of a Software Pipeline. *Proteins: Struct., Funct., Bioinf.* **2005**, *59*, 687-96.
57. Mulder, F.A.A.; Schipper D.; Bott, R.; Boelens, R. Altered flexibility in the substrate-binding site of related native and engineered high-alkaline *Bacillus subtilis*ins. *J. Mol. Biol.* **1999**, *292*, 111-123.
58. Vandenameele, J.; Lejeune, A.; Di Paolo, A.; Brans, A.; Frère, J.M.; Schmid, F.X.; Matagne, A. Folding of class A β -Lactamase is Rate-limited by Peptide Bond Isomerization and Occurs via Parallel Pathways. *Biochemistry* **2010**, *49*, 4264-4275.
59. Santoro, M.M.; Bolen, D. W. Unfolding Free Energy Changes Determined by the Linear Extrapolation Method. 1. Unfolding of Phenylmethanesulfonyl Alpha-Chymotrypsin Using Different Denaturants. *Biochemistry* **1988**, *27*, 8063-8068.
60. Pace, C.N. Measuring and Increasing Protein Stability. *Trends Biotechnol.* **1990**, *8*, 93-98.
61. Dumoulin, M.; Conrath, K.; Van Meirhaeghe, A.; Meersman, F.; Heremans, K.; Frenken, L. G.; Muyldermans, S.; Wyns, L.; and Matagne, A. Single-domain Antibody Fragments with High Conformational Stability. *Protein Sci.* **2002**, *11*, 500-515.
62. Redfield, C. Molten Globules. *Curr. Biol.* **1999**, *9*, R313
63. Kuwajima, K. The Molten Globule State as a Clue for Understanding the Folding and Cooperativity of Globular-Protein Structure. *Prot. Struct. Funct. Gen.* **1989**, *6*, 87-103.
64. Ptitsyn, O.B.; Pain, R.H.; Semisotnov, G.V.; Zerovnik, E.; Razgulyaev, O.I. Evidence for a Molten Globule State as a General Intermediate in Protein Folding. *FEBS Lett.* **1990**, *262*, 20-24.
65. Semisotnov, G.V.; Rodionova, N.A.; Razgulyaev, O.I.; Uversky, V.N.; Gripas, A.F.; Gilmanshin, R.I. Study of the "Molten Globule" Intermediate State in Protein Folding by a Hydrophobic Fluorescent Probe. *Biopolymers* **1991**, *31*, 119-128.
66. Kim, Y.; Cunningham, M.A.; Mire, J.; Tesar, C.; Sacchettini, J.; Joachimiak, A. NDM-1, the Ultimate Promiscuous Enzyme: Substrate Recognition and Catalytic Mechanism. *FASEB J.* **2013**, *27*, 1917-1927.
67. Eftink, M.; Ghiron, C.A. Fluorescence Quenching Studies with Proteins. *Anal. Biochem.* **1981**, *114*, 119-227
68. Karsisiotis, A.I.; Damblon, C.F.; Roberts, G.C.K. Complete ^1H , ^{15}N , and ^{13}C Resonance Assignments of *Bacillus cereus* Metallo- β -lactamase and its Complex with the Inhibitor R-Thiomandelic Acid. *Biomol. NMR Assign.* **2014**, *8*, 313-318.
69. Hubbard, S.J.; Thornton, J.M. 'NACCESS', Computer Program, Department of Biochemistry and Molecular Biology, University College London, 1993.
70. Rasia, R.M.; Vila, A.J. Structural Determinants of Substrate Binding to *Bacillus cereus* Metallo- β -lactamase. *J. Biol. Chem.* **2004**, *279*, 26046-26051.
71. Jacquin, O. (2011) *Etude des propriétés de repliement et de fixation du zinc de la métallo- β -lactamase BclII de Bacillus cereus 569/H/9*. Ph.D. thesis, University of Liège
72. Myers, J.K.; Pace, C.N.; Scholtz, J.M. Denaturant m Values and Heat Capacity Changes: Relation to Changes in Accessible Surface Areas of Protein Unfolding. *Protein Sci.* **1995**, *4*, 2138-2148.
73. Pfeil, W. Protein Stability and Folding: a Collection of Thermodynamic Data; Springer-Verlag Berlin, Heidelberg, GmbH, 1998.

74. Whitford, D. Proteins: Structure and Function; John Wiley & Sons, Ltd., 2005.
75. Creighton, T.E. The Biophysical Chemistry of Nucleic Acids and Proteins, Helvetian Press, 2010.
76. Lehninger, A.L.; Nelson, D.L.; Cox, M.M. Principles of Biochemistry, 6th edition. Freeman W.H. and Company, New York, 2013.
77. Palm-Espling, M.E.; Niemiec, M.S.; Wittung-Stafshede, P. Role of Metal in Folding and Stability of Copper Proteins *in vitro*. *Biochim. Biophys. Acta* **2012**, *1823*, 1594-1603.
78. Wittung-Stafshede P. Role of Cofactors in Protein Folding. *Acc. Chem. Res.* **2002**, *35*, 201-208.
79. Selevsek, N.; Rival, S.; Tholey, A.; Heinzle, E.; Heinz, U.; Hemmingsen, L.; Adolph, H.W. Zinc Ion-induced Domain Organization in Metallo- β -Lactamases. *J. Biol. Chem.* **2009**, *284*, 16419-16431.
80. Lassaux, P.; Traoré, D.A.; Loisel, E.; Favier, A.; Docquier, J.D.; Sohier, J.S.; Laurent, C.; Bebrone, C.; Frère, J.M.; Ferrer, J.L.; Galleni, M. Biochemical and Structural Characterization of the Subclass B1 Metallo- β -lactamase VIM-4. *Antimicrob. Agents Chemother.* **2011**, *55*, 1248-1255.
81. Dragani, B.; Cocco, R.; Ridderström, M.; Stenberg, G.; Mannervik, B.; Aceto, A. Unfolding and Refolding of Human Glyoxalase II and its Single-tryptophan Mutants. *J. Mol. Biol.* **1999**, *291*, 481-490.
82. Concha, N.O.; Rasmussen, B.A.; Bush, K.; and Herzberg, O. Crystal Structure of the Wide-spectrum Binuclear Zinc β -Lactamase from *Bacteroides fragilis*. *Structure* **1996**, *4*, 823-836.
83. Concha, N.O.; Janson, C.A.; Rowling, P.; Pearson, S.; Cheever, C.A.; Clarke, B.P.; Lewis, C.; Galleni, M.; Frère, J.M.; Payne, D.J.; Bateson, J.H.; Abdel-Meguid, S.S. Crystal Structure of the IMP-1 Metallo β -Lactamase from *Pseudomonas aeruginosa* and its Complex with a Mercaptocarboxylate Inhibitor: Binding Determinants of a Potent, Broad-spectrum Inhibitor, *Biochemistry* **2000**, *39*, 4288-4298.
84. Fitzgerald, P.M.; Wu, J.K.; Toney, J.H. Unanticipated Inhibition of the Metallo- β -lactamase from *Bacteroides fragilis* by 4-Morpholineethanesulfonic Acid (MES): a Crystallographic Study at 1.85-Å Resolution, *Biochemistry* **1998**, *37*, 6791-6800.
85. Toney, J.H.; Fitzgerald, P.M.; Grover-Sharma, N.; Olson, S.H.; May, W.J.; Sundelof, J.G.; Vanderwall, D.E.; Cleary, K.A.; Grant, S.K.; Wu, J.K.; Kozarich, J.W.; Pompliano, D.L.; Hammond, G.G. Antibiotic Sensitization Using Biphenyl Tetrazoles as Potent Inhibitors of *Bacteroides fragilis* Metallo- β -lactamase, *Chem. Biol.* **1998**, *5*, 185-196.
86. Toney, J.H.; Hammond, G.G.; Fitzgerald, P.M.; Sharma, N.; Balkovec, J.M.; Rouen, G.P.; Olson, S.H.; Hammond, M.L.; Greenlee, M.L.; Gao, Y.D. Succinic Acids as Potent Inhibitors of Plasmid-borne IMP-1 Metallo- β -lactamase, *J. Biol. Chem.* **2001**, *276*, 31913-31918.
87. Scrofani, S.D.B.; Chung, J.; Huntley, J.J.A.; Benkovic, S.J.; Wright, P.E.; and Dyson, H.J. NMR Characterization of the Metallo- β -lactamase from *Bacteroides fragilis* and its Interaction with a Tight-binding Inhibitor: role of an Active-site Loop. *Biochemistry* **1999**, *38*, 14507-14514.
88. Yang, Y.; Keeney, D.; Tang, X.J.; Canfield, N.; and Rasmussen, B.A. Kinetic Properties and Metal Content of the Metallo- β -lactamase CcrA Harboring Selective Amino acid Substitutions. *J. Biol. Chem.* **1999**, *274*, 15706-15711.
89. Huntley, J.J.; Scrofani, S.D.B.; Osborne, M.J.; Wright, P.E.; Dyson, H.J. Dynamics of the Metallo- β -Lactamase from *Bacteroides fragilis* in the Presence and Absence of a Tight-binding Inhibitor. *Biochemistry* **2000**, *39*, 13356-13364.

90. Huntley, J.J.; Fast, W.; Benkovic, S.J.; Wright, P.E.; Dyson, H.J. Role of a Solvent-Exposed Tryptophan in the Recognition and Binding of Antibiotic Substrates for a Metallo- β -lactamase. *Protein Sci.* **2003**, *12*, 1368–1375.
91. Mollard, C.; Moali, C.; Papamichael, C.; Damblon, C.; Vessilier, S.; Amicosante, G.; Schofield, C.J.; Gelleni, M.; Frère, J.M.; and Roberts, G.C.K. Thiomandelic Acid, a Broad Spectrum Inhibitor of Zinc β -Lactamases. *J. Biol. Chem.* **2001**, *276*, 45015-45023.
92. Payne, D.J.; Hueso-Rodríguez, J.A.; Boyd, H.; Concha, N.O.; Janson, C.A.; Gilpin, M.; Bateson, J.H.; Cheever, C.; Niconovich, N.L.; Pearson, S.; Rittenhouse, S.; Tew, D.; Díez, E.; Pérez, P.; De La Fuente, J.; Rees, M.; Rivera-Sagredo, A. Identification of a Series of Tricyclic Natural Products as Potent Broad-spectrum Inhibitors of Metallo- β -lactamases. *Antimicrob. Agents Chemother.* **2002**, *46*, 1880-1886.
93. Docquier, J.D.; Lamotte-Brasseur, J.; Galleni, M.; Amicosante, G.; Frère, J.M.; Rossolini, G.M. On Functional and Structural Heterogeneity of VIM-type Metallo- β -lactamases. *J. Antimicrob. Chemother.* **2003**, *51*, 257-266.
94. Moali, C.; Anne, C.; Lamotte-Brasseur, J.; Gros Lambert, S.; Devreese, B.; Van Beeumen, J.; Galleni, M.; and Frère, J.M. (2003) Analysis of the Importance of the Metallo- β -lactamase Active Site Loop in Substrate Binding and Catalysis. *Chem. Biol.* **2003**, *10*, 319-329.
95. Krauss, M.; Gresh, N.; Antony, J. (2003) Binding and Hydrolysis of Ampicillin in the Active Site of a Zinc Lactamase. *J. Phys. Chem. B* **2003**, *107*, 1215-1229.
96. Tomatis, P.E.; Fabiane, S.M.; Simona, F.; Carloni, P.; Sutton, B.J.; Vila, A.J. Adaptive Protein Evolution Grants Organismal Fitness by Improving Catalysis and Flexibility. *Proc. Natl. Acad. Sci. U.S.A.* **2008**, *105*, 20605-20610.
97. Salsbury, F.R.; Crowder, M.W.; Kingsmore, S.F.; Huntley, J.J. Molecular Dynamic Simulations of the Metallo- β -lactamase from *Bacteroides fragilis* in the Presence and Absence of a Tight-binding Inhibitor. *J. Mol. Model.* **2009**, *15*, 133-145.
98. González, J.M.; Buschiazzo, A.; Vila, A.J. Evidence of Adaptability in Metal Coordination Geometry and Active-Site Loop Conformation among B1 Metallo- β -lactamases. *Biochemistry* **2010**, *49*, 7930-7938.
99. Valdez, C.E.; Sparta, M.; Alexandrova, A.N. The Role of the Flexible L43-S54 Protein Loop in the CcrA Metallo- β -lactamase in Binding Structurally Dissimilar β -Lactam Antibiotics. *J. Chem. Theory Comput.* **2013**, *9*, 730–737.
100. Rydzik, A.M.; Brem, J.; van Berkel, S.S.; Pfeffer, I.; Makena, A.; Claridge, T.D.; Schofield, C.J. Monitoring Conformational Changes in the NDM-1 Metallo- β -lactamase by 19F NMR Spectroscopy. *Angew. Chem. Int. Ed. Engl.* **2014**, *53*, 3129-3133.
101. Zhang, H.; Hao, Q. Crystal Structure of NDM-1 Reveals a Common β -Lactam Hydrolysis Mechanism, *FASEB J.* **2011**, *25*, 2574-2582.
102. King, D.T.; Worrall, L.J.; Gruninger, R.; Strynadka, N.C. New Delhi Metallo- β -lactamase: Structural Insights into β -Lactam Recognition and Inhibition. *J. Am. Chem. Soc.* **2012**, *134*, 11362-11365.

FOOTNOTE

This work was supported in part by grants of the National Fund for Scientific Research (F.R.S.-FNRS, Belgium; Fonds de la Recherche Fondamentale et Collective, contract numbers 2.4550.05 and 2.4530.09) and by the Belgian program of Interuniversity Attraction Poles initiated by the Federal Office for Scientific Technical and Cultural Affairs (PAI n° P5/33, P6/19 and P7/44).

Some NMR experiments in Oxford were collected with access provided by the European Commission's Framework Program 7 (FP7) East-NMR (contract number 228461) and BioNMR projects (contract number 261863).

The abbreviations used are: BcII, β -lactamase II from *Bacillus cereus* 569/H/9; CD, circular dichroism; GdmCl, guanidinium chloride; MBL, metallo β -lactamase; ANS, 1-anilino-8-naphthalenesulfonate; HSQC, heteronuclear single quantum coherence; CSP, combined chemical shift perturbation.

TABLE LEGENDS

TABLE 1. Thermodynamic parameters for GdmCl- and urea-induced unfolding transition of apoBcII.

TABLE 2. Thermodynamic parameters for GdmCl-induced unfolding transition of holoBcII.

FIGURE LEGENDS

FIGURE 1. Schematic ribbon representation of the structure of BcII 569/H/9 (1BVT (40)). The zinc ions at the catalytic site are represented as yellow spheres, α -helices and β -strands are shown in red and blue, respectively, and the four tryptophan residues are labelled and coloured green. The β 3- β 4 and β 11- α 4 loops [residues 32-38(59-66) and 170-188(223-241), respectively] are also indicated. The figure was generated using the open-source molecular graphics system PyMol (The PyMOL Molecular Graphics System, Version 1.2r3pre, Schrödinger, LLC).

FIGURE 2. Fluorescence (A,B) and far-UV CD (C,D) spectra of native ([GdmCl] = 0 M, thick line), partially folded ([GdmCl] = 2.4 M, dashed line) and unfolded ([GdmCl] = 4 M, thin line) forms of holo (A,C) and apo (B,D) BcII. GdmCl-induced equilibrium unfolding transitions of holo (E) and apo (F) BcII at pH 7.5 and 25°C, monitored by the change in fluorescence intensity at 370 nm (\square), CD at 222 nm (\circ) and enzyme activity (Δ ; holoBcII only); the filled squares (\blacksquare) correspond to the refolding of BcII after 12 h incubation in 6 M GdmCl, monitored by the change in fluorescence intensity at 370 nm. Data are shown as the fractional change in signal (58) at each GdmCl concentration; they were analysed on the basis of two- and three-state models for apo and holoBcII, respectively, and the solid lines represent the best fit calculated using the thermodynamic values in Tables 1 and 2, respectively. The curve for holoBcII unfolding followed by activity measurements is there to guide the eye only.

FIGURE 3. 2D ^1H - ^{15}N HSQC spectra for histidine imidazole observation. (A) Superimposition of data obtained for native BcII in the presence (holoBcII, in red) and absence (apoBcII, in blue) of zinc ions, with no GdmCl; (B) Superimposition of signals observed for holoBcII in the presence of 0 M (blue), 2.25 M (red) and 2.5 M (green) GdmCl. Note that standard BBL numbering system only is used.

FIGURE 4. Stern-Volmer plots of holoBcII tryptophan fluorescence, in the presence of 0.1 mM ZnSO_4 , quenched by acrylamide at several GdmCl concentrations. Experiments were performed for the native state in the absence of GdmCl (\square), the intermediate state in the presence of 2.4 M GdmCl (\circ) and the unfolded state in the presence of 3.5 M GdmCl (∇). Data are the average of at least 3 independent experiments and error bars represent standard deviations.

FIGURE 5. 2D ^1H - ^{15}N HSQC spectra of holoBcII in the presence of various GdmCl concentrations. A: [GdmCl] = 0 M; B: [GdmCl] = 1.63 M; C: [GdmCl] = 2.34 M; D: [GdmCl] = 4.0 M. Plots have been drawn using CcpNmr Analysis (56).

FIGURE 6. Overlay of 2D ^1H - ^{15}N HSQC spectra of holoBcII in the presence of various GdmCl concentrations: 0 M (black); 1 M (green); 1.6 M (blue) and 2.34 M (pink). Arrows indicate shifts and their directions, circles are for peaks corresponding to the unfolded protein in 2.34 M GdmCl, and arcs indicate non-linear CSPs. Residues are numbered as in the sequence, i.e. Lys104(135), Lys134(181), Lys 227(291).

FIGURE 7. (A) Combined chemical shift perturbations (CSPs) between 0 and 2.34 M GdmCl, calculated using equation (2) and shown as histograms versus the BcII amino acid sequence. The dashed line represents the threshold (0.064 ppm) for significant chemical shift perturbations calculated as described in Materials and Methods. With residues Ile83(113), Glu151(198), Val165(218), Lys176(229), estimation of the CSPs was done by linear extrapolation. Those 8 residues [Lys50(78), Thr64(92), Glu72(100), Ile83(113), Ala115(146), Thr131(178), Val165(218), Glu188(243)] whose signals disappeared completely as GdmCl concentration was increased above 0.75 M (see text) are indicated by asterisk. Sequence elements corresponding to loops β 3- β 4 and β 11- α 4 are indicated; (B) Schematic ribbon representation of the structure where green areas represent those residues undergoing significant CSPs.

FIGURE 8. Influence of GdmCl on the indole side chain (A) and backbone amide (B) resonances of the four tryptophan residues of holoBcII. The combined chemical shift perturbation (CSP) for sidechain $\text{H}\epsilon$ 1- $\text{N}\epsilon$ 1 (A) and backbone H-N peaks (B) plotted as a function of GdmCl concentration. The solvent accessibility of the corresponding side and main chains, as computed with NACCESS (69), is indicated.

FIGURE 9. 2D ^1H - ^{15}N HSQC spectra for histidine imidazole of BcII in the presence of 2 M GdmCl. (A) holoBcII, (B) apoBcII, (C) Zn/apoBcII molar ratio = 1, and (D) Zn/apoBcII molar ratio = 2. Note that standard BBL numbering system only is used.

Table 1

	GdmCl			Urea		
	$\Delta G^{\circ}_{\text{NU}}$ (kJ·mol ⁻¹)	$-m_{\text{NU}}$ (kJ·mol ⁻¹ ·M ⁻¹)	C_{m} (M)	$\Delta G^{\circ}_{\text{NU}}$ (kJ·mol ⁻¹)	$-m_{\text{NU}}$ (kJ·mol ⁻¹ ·M ⁻¹)	C_{m} (M)
Intrinsic fluorescence	33 ± 1.4	21 ± 1	1.5 ± 0.2	33 ± 1	10 ± 0.4	3.3 ± 0.3
Far-UV CD	28 ± 2	19.4 ± 1.3	1.5 ± 0.2	32 ± 1.3	9.7 ± 0.4	3.3 ± 0.3

Table 2

	$\Delta G^{\circ}_{\text{NI}}$ (kJ·mol ⁻¹)	$-m_{\text{NI}}$ (kJ·mol ⁻¹ ·M ⁻¹)	$(C_{\text{m}})_{\text{NI}}$ (M)	$\Delta G^{\circ}_{\text{IU}}$ (kJ·mol ⁻¹)	$-m_{\text{IU}}$ (kJ·mol ⁻¹ ·M ⁻¹)	$(C_{\text{m}})_{\text{IU}}$ (M)
Intrinsic fluorescence	29 ± 6	15 ± 3	1.9 ± 0.8	66 ± 3	24 ± 1	2.8 ± 0.3
Far-UV CD	15 ± 3	8 ± 2	1.9 ± 0.8	64 ± 4	23 ± 1.4	2.7 ± 0.3

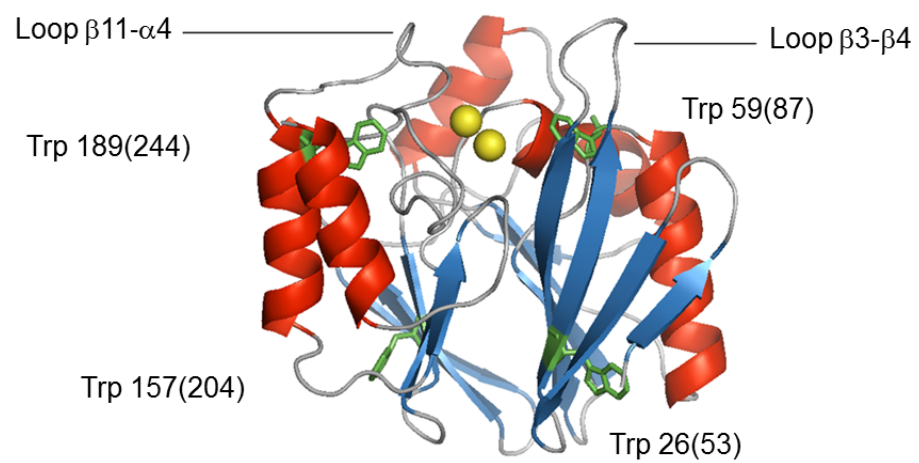


Figure 1

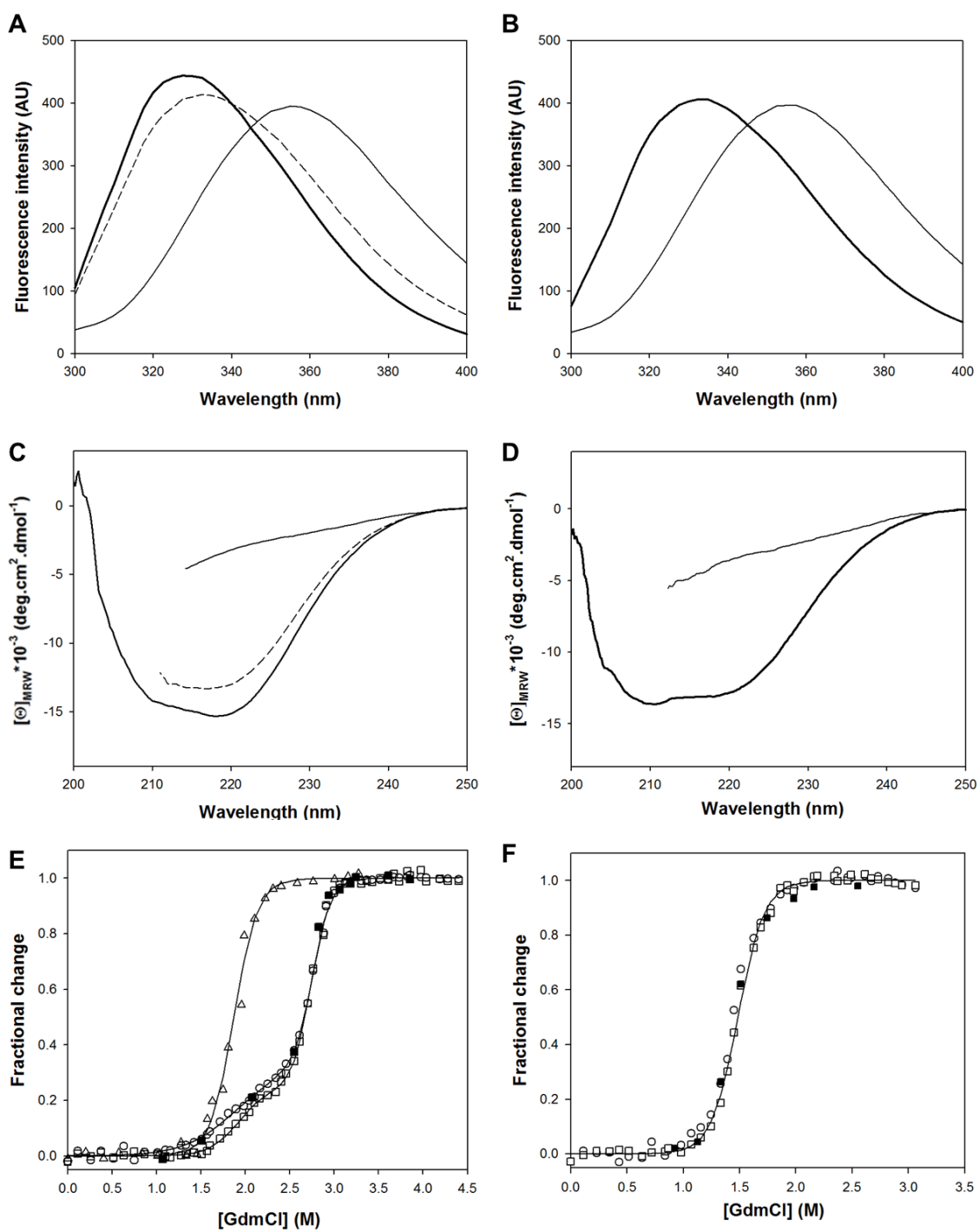


Figure 2

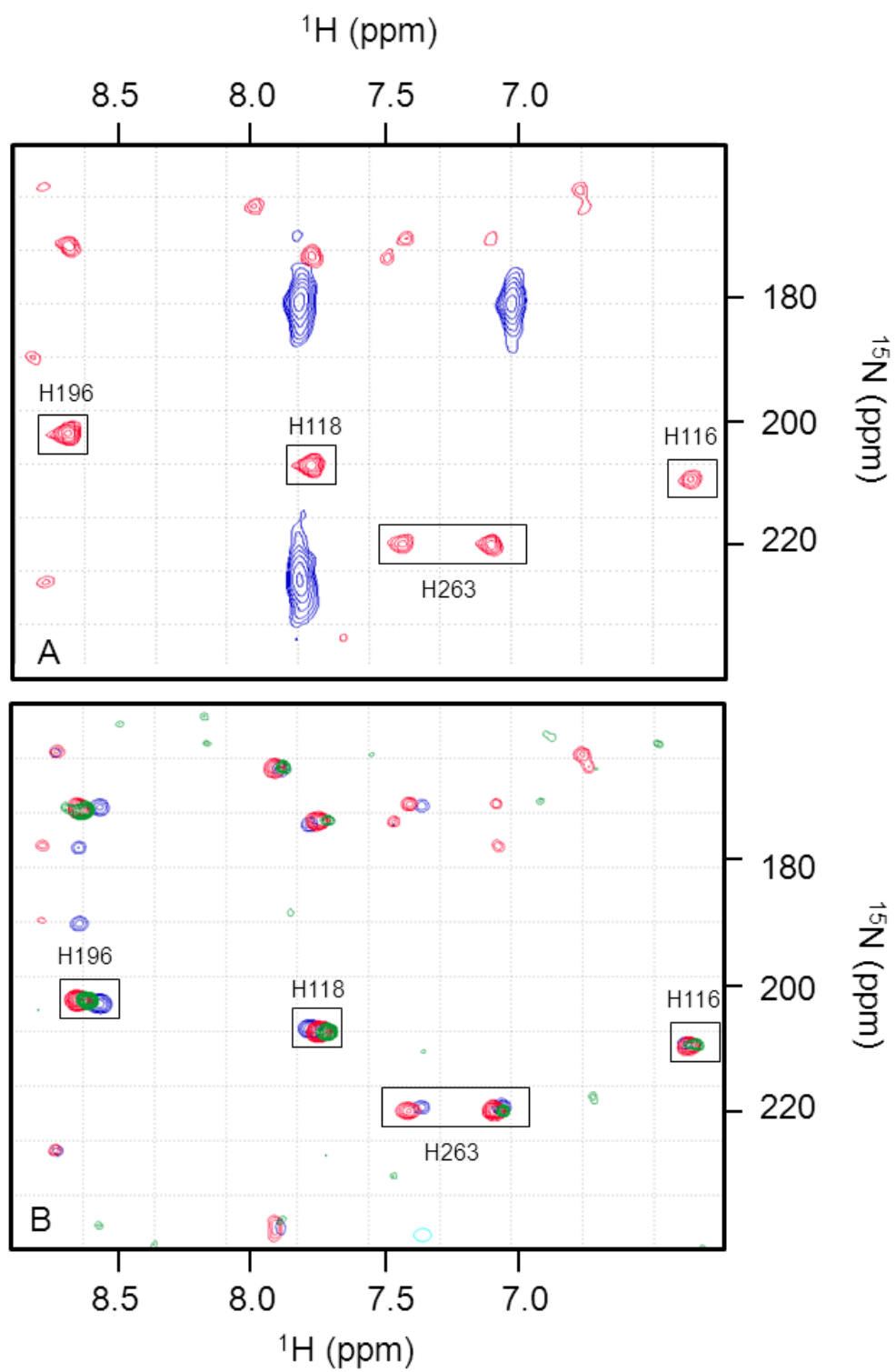


Figure 3

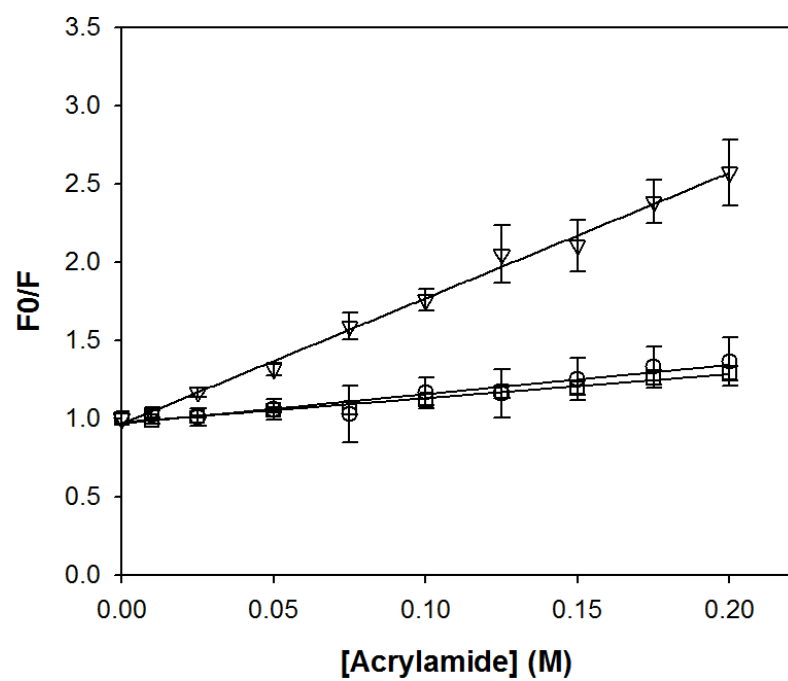


Figure 4

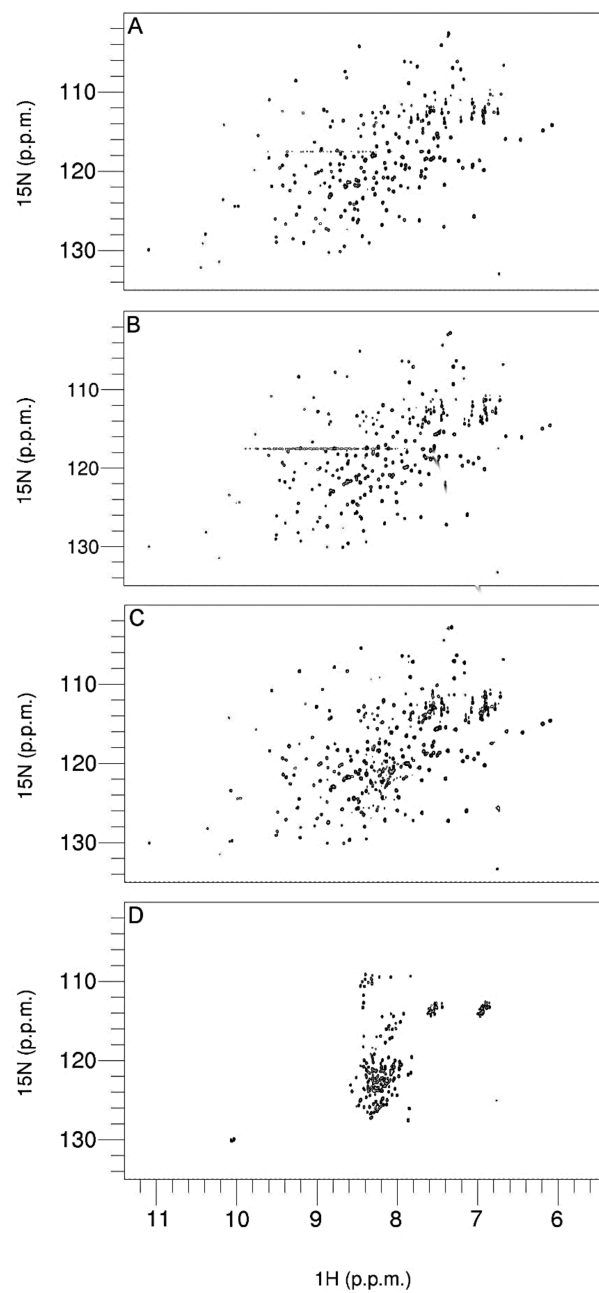


Figure 5

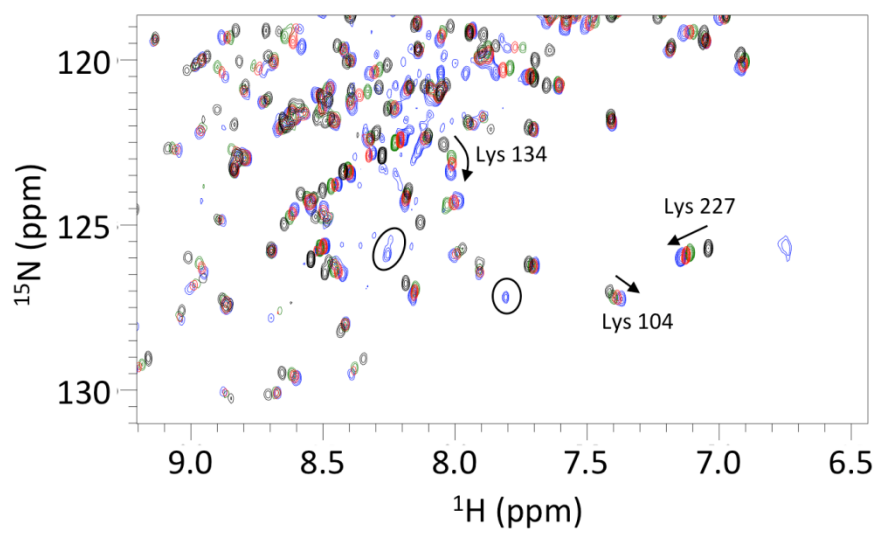


Figure 6

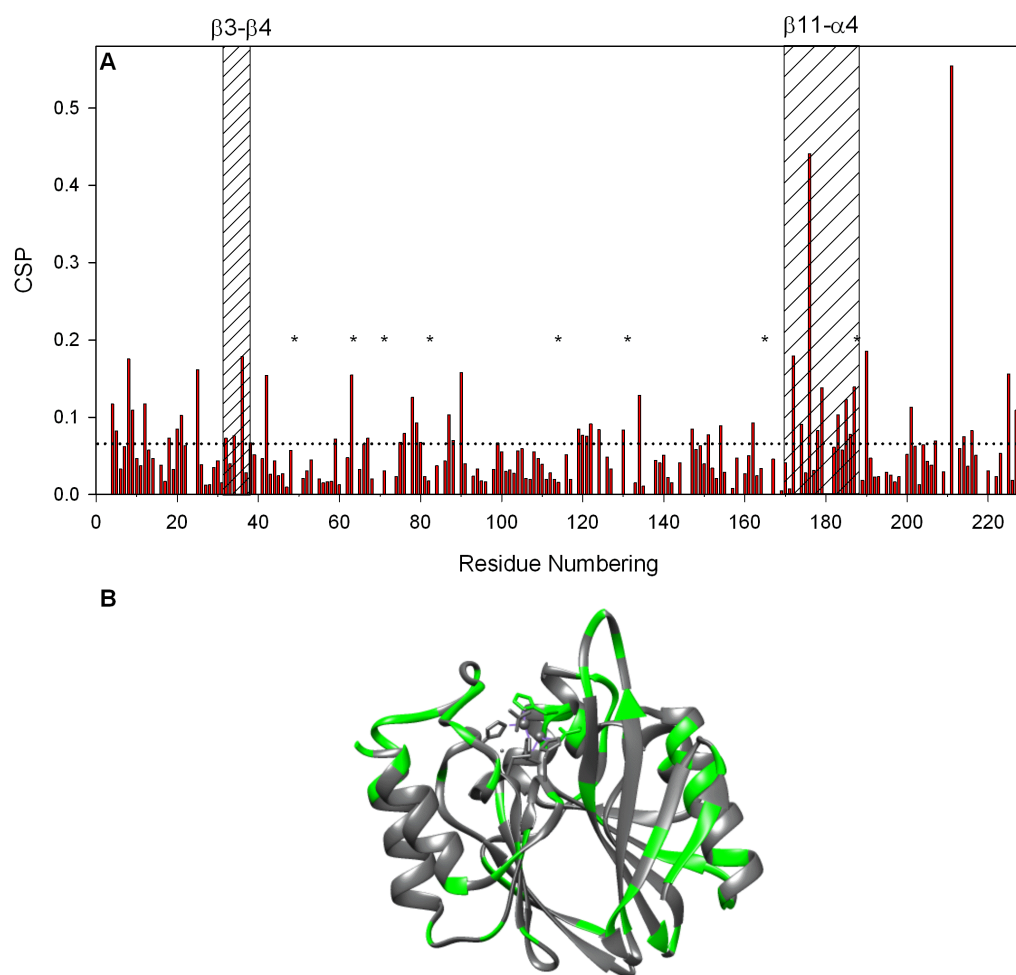


Figure 7

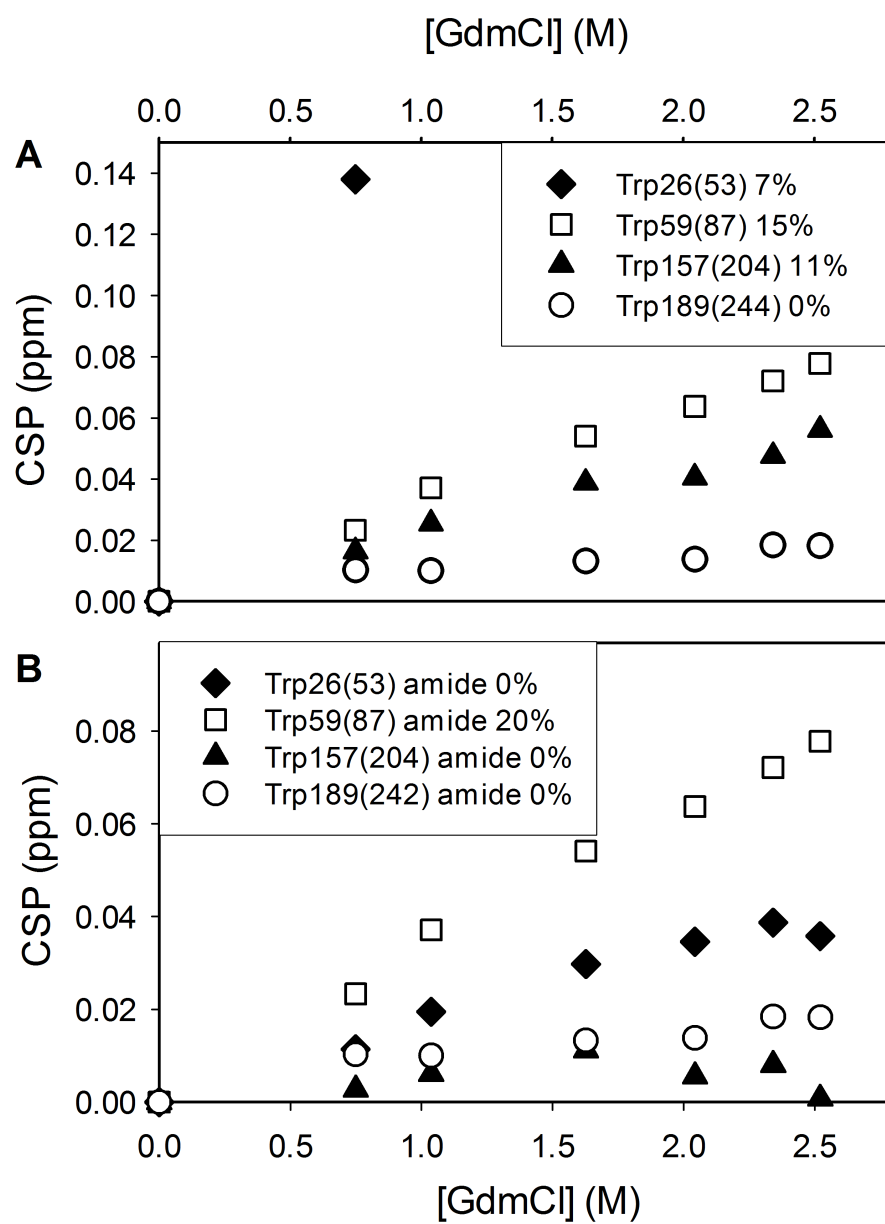


Figure 8

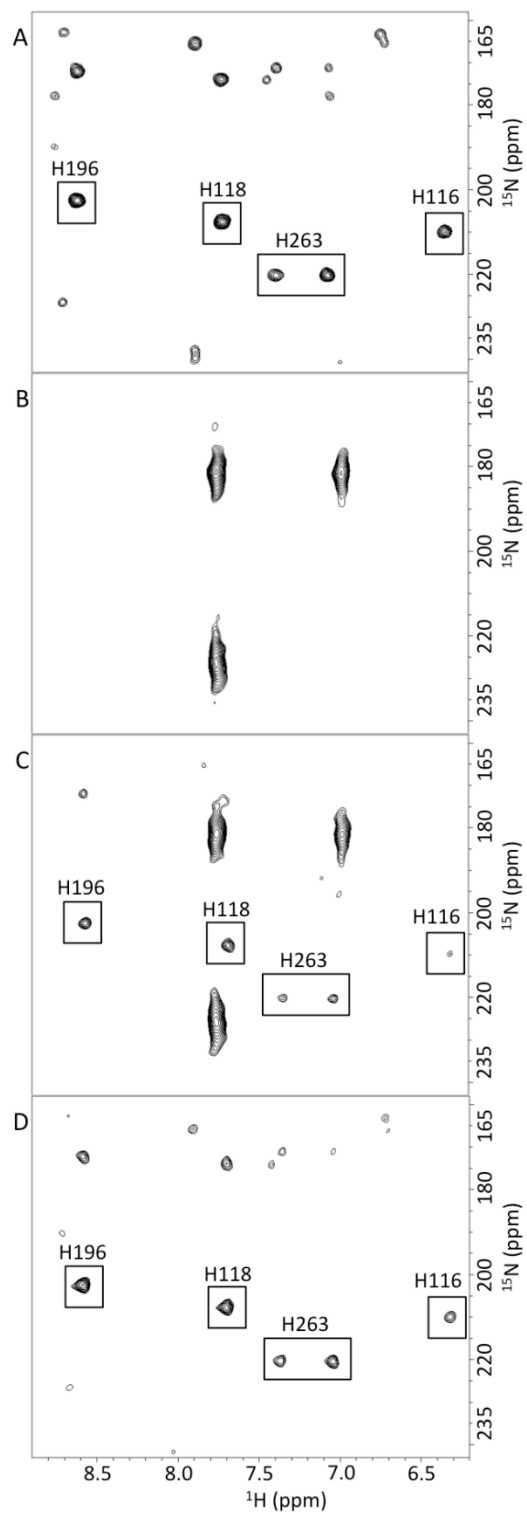


Figure 9

TABLE S1: selection of 50 residues buried in the protein core. Their side chain and main chain relative solvent accessibility were computed with NACCESS (68) and their CSPs are given for both GdmCl and urea concentrations in the range of 0 and 2.34 M, and 0 and 7.9 M, respectively. “—” residues which peaks could not be monitored in the NMR experiment.

<i>Residue</i>	<i>Seq.#</i>	<i>MBL#</i>	<i>Total Side Rel. Solvent Access.</i>	<i>Main Chain. Rel. Solvent Access.</i>	<i>CSP GdmCl (0-2.34 M)</i>	<i>CSP Urea (0- 7.9 M)</i>
ILE	16	43	0	0	0.0383	--
VAL	25	52	0	0	0.1618	0.06309
TRP	26	53	7.1	0	0.0387	0.03486
HIS	28	55	0.4	0	0.013	0.0371
GLU	30	57	0.6	0	0.0439	0.02328
GLY	43	71	0.1	0	0.0262	0.03661
LEU	44	72	0	0	0.0437	--
VAL	45	73	0	0	0.0245	--
LEU	46	74	0	0	0.0272	0.02555
LEU	52	80	0	0	0.031	0.03203
VAL	53	81	0.4	0	0.045	0.07101
VAL	55	83	0	0	0.0154	0.02993
ASP	56	84	0.8	0	--	0.01915
SER	58	86	0.1	0	0.0172	0.01395
LEU	63	91	11.3	0	0.1545	0.13038
LEU	67	95	0	0	0.0732	--
ILE	68	96	0.5	0	0.0206	0.07411
VAL	71	99	0	0	0.031	0.04982
ASP	81	111	8.8	0	0.0235	0.01339
VAL	82	112	0	0	0.0176	0.1693
HIS	86	116	0.5	0	0.0436	0.05328
ARG	91	121	1.2	0	0.0399	0.01336
GLY	94	124	0	0	0.0335	0.0181
ILE	95	125	2.2	0	0.0176	0.01116
LEU	98	128	0	0	0.0325	0.02221
HIS	106	137	9.9	0	0.0209	0.02619
SER	107	138	0	0	0.0198	--

THR	111	142	0.4	0	0.0198	0.01048
ALA	112	143	8	0	0.0283	0.0574
LEU	114	145	21.5	0	0.0162	--
ALA	115	146	0	0	--	0.02364
PHE	135	182	13.8	0	0.0112	0.02869
GLU	141	188	11.3	0	0.0222	0.04759
GLY	148	195	0	0	0.0586	0.02227
THR	150	197	5.6	0	0.0399	0.03489
ASN	153	200	1.7	0	0.0211	0.03633
VAL	156	203	0	0	--	0.01667
LEU	158	205	0.1	0	0.0474	0.06348
ILE	163	216	7.3	0	0.0246	0.04554
LEU	164	217	0	0	0.0337	0.03932
LYS	171	224	17.2	0	0.00751	--
TRP	189	244	0	0	0.0184	--
SER	192	247	3.3	0	0.0227	0.07171
ILE	193	248	0	0	0.0232	0.0077
VAL	196	251	0	0	0.0253	0.04009
LEU	197	252	4.3	0	0.0165	0.0528
ALA	205	258	21.3	0	0.043	0.1008
VAL	206	259	0	0	0.0384	0.11638
VAL	207	260	0.4	0	0.0695	0.06098
THR	222	303	0	0	0.0237	0.04802

Table S1